Simulation and observations of stratospheric aerosols from the 2009 Sarychev volcanic eruption

Ben Kravitz,[1,2] Alan Robock,[1] Adam Bourassa,[3] Terry Deshler,[4] Decheng Wu,[5,6] Ina Mattis,[7] Fanny Finger,[7] Anne Hoffmann,[8] Christoph Ritter,[8] Lubna Bitar,[9,10] Thomas J. Duck,[9] and John E. Barnes[11]

Received 13 December 2010; revised 26 June 2011; accepted 7 July 2011; published 30 September 2011.

[1] We used a general circulation model of Earth's climate to conduct simulations of the 12–16 June 2009 eruption of Sarychev volcano (48.1°N, 153.2°E). The model simulates the formation and transport of the stratospheric sulfate aerosol cloud from the eruption and the resulting climate response. We compared optical depth results from these simulations with limb scatter measurements from the Optical Spectrograph and Infrared Imaging System (OSIRIS), in situ measurements from balloon-borne instruments lofted from Laramie, Wyoming (41.3°N, 105.7°W), and five lidar stations located throughout the Northern Hemisphere. The aerosol cloud covered most of the Northern Hemisphere, extending slightly into the tropics, with peak backscatter measured between 12 and 16 km in altitude. Aerosol concentrations returned to near-background levels by spring 2010. After accounting for expected sources of discrepancy between each of the data sources, the magnitudes and spatial distributions of aerosol optical depth due to the eruption largely agree. In conducting the simulations, we likely overestimated both particle size and the amount of SO_2 injected into the stratosphere, resulting in modeled optical depth values that were a factor of 2–4 too high. Modeled optical depth due to the eruption shows a peak too late in high latitudes and too early in low latitudes, suggesting a problem with stratospheric circulation in the model. The model also shows a higher decay rate in optical depth than is observed, showing an inaccuracy in stratospheric removal rates in some seasons. The modeled removal rate of sulfate aerosols from the Sarychev eruption is higher than the rate calculated for aerosols from the 1991 eruption of Mt. Pinatubo.

Citation: Kravitz, B., et al. (2011), Simulation and observations of stratospheric aerosols from the 2009 Sarychev volcanic eruption, *J. Geophys. Res.*, *116*, D18211, doi:10.1029/2010JD015501.

1. Introduction

[2] Sarychev volcano (48.1°N, 153.2°E) in the Kuril Islands erupted (Figure 1) over the period 12–16 June 2009, injecting approximately 1.2 Tg of sulfur dioxide into the lower stratosphere at an altitude of approximately 11–16 km [*Haywood et al.*, 2010]. This was the second major stratospheric injection of SO_2 in the span of a year, the previous one being the eruption of Kasatochi on 8 August 2008 [*Kravitz and Robock*, 2011]. The largest eruptions immediately prior to these were Mount Pinatubo and Mount Hudson in 1991 (S. Carn and A. Krueger, 2004, TOMS Volcanic Emissions Group, http://toms.umbc.edu/Images/Mainpage/toms_so2chart_color.jpg).

[3] The climate effects of volcanic eruptions are well established [*Robock*, 2000]. These effects are due to the production of a layer of sulfate aerosols in the stratosphere, which efficiently backscatters solar radiation, effectively increasing the planetary albedo and causing cooling at the surface. For these radiative effects to accumulate, the aerosols must remain in the atmosphere for an extended period of time. Stratospheric volcanic aerosols have an average *e*-folding lifetime of 1 year [*Budyko*, 1977; *Stenchikov et al.*,

[1]Department of Environmental Sciences, Rutgers University, New Brunswick, New Jersey, USA.
[2]Now at Department of Global Ecology, Carnegie Institution for Science, Stanford, California, USA.
[3]Department of Physics and Engineering Physics, University of Saskatchewan, Saskatoon, Saskatchewan, Canada.
[4]Department of Atmospheric Science, University of Wyoming, Laramie, Wyoming, USA.
[5]Key Laboratory of Atmospheric Composition and Optical Radiation, Chinese Academy of Sciences, Hefei, China.
[6]Anhui Institute of Optics and Fine Mechanics, Chinese Academy of Sciences, Hefei, China.
[7]Leibniz Institute for Tropospheric Research, Leipzig, Germany.
[8]Alfred Wegener Institute for Polar and Marine Research in the Helmholtz Association, Potsdam, Germany.
[9]Department of Physics and Atmospheric Science, Dalhousie University, Halifax, Nova Scotia, Canada.
[10]Meteorological Service of Canada, Montreal, Quebec, Canada.
[11]Mauna Loa Observatory, National Oceanic and Atmospheric Administration Earth System Research Laboratory, Hilo, Hawaii, USA.

0148-0227/11/2010JD015501

Figure 1. The eruption of Sarychev volcano on 12 June 2009 as seen from the International Space Station (Sarychev Peak Eruption, Kuril Islands: Natural Hazards, 2009, NASA Earth Observatory, astronaut photograph ISS020-E-9048, http://earthobservatory.nasa.gov/NaturalHazards/view.php?id=38985). Image courtesy of the Image Science & Analysis Laboratory, NASA Johnson Space Center.

1998; *Gao et al.*, 2007]. Were the injection to occur only into the troposphere, the climate effects would be greatly muted, as the atmospheric lifetime of tropospheric aerosols is about 1 week [*Seinfeld and Pandis*, 2006].

[4] Determining the climate effects requires an accurate assessment of the amount of sulfate aerosols created in the stratosphere, as well as the spatial and temporal patterns of the aerosol layer. General circulation models are useful predictive tools for estimating volcanic effects, and they have been used with great success in replicating the effects of past volcanic eruptions [e.g., *Oman et al.*, 2006a]. However, any model can benefit from further testing and improvement. As such, we use the recent eruption of Sarychev to test the model's ability to accurately create and transport sulfate aerosols.

[5] *Kravitz et al.* [2010] compared modeled results of sulfate aerosol optical depth with satellite and ground-based retrievals from the Kasatochi eruption. Although the spatial pattern of aerosol distributions in the model and the observations largely agreed, they discovered a discrepancy of an order of magnitude in the actual values. They were able to explain some of this discrepancy, but a factor of 2–4 remained unexplained. A similar comparison between model results and observations of the eruption of Sarychev will allow us to expand this study and better analyze the discrepancy. As in the study by *Kravitz et al.* [2010], a large part of our comparison will be with data from the Optical Spectrograph and Infrared Imaging System (OSIRIS), a Canadian instrument on the Swedish satellite Odin [*Llewellyn et al.*, 2004]. Launched in 2001 and still operational, OSIRIS measures the vertical profile of limb-scattered sunlight spectra. Previous work has demonstrated the capability of retrieving information about the vertical distribution of stratospheric aerosol from limb scatter measurements [*Bourassa et al.*, 2007, 2008a; *Rault and Loughman*, 2007; *Tukiainen et al.*, 2008].

[6] Our second means of comparison is with in situ measurements of aerosol size and concentration from balloon-borne instruments that are launched three or four times per year from Laramie, Wyoming (41.3°N, 105.7°W). Past use of this very long-term data set in analyzing volcanic aerosol layers in the stratosphere is well established [e.g., *Deshler et al.*, 2006]. We suspect one of the main sources of discrepancy by *Kravitz et al.* [2010] was inaccurate estimation of aerosol size, which would have a significant impact on our determination of aerosol optical depth, as we describe in section 3. Direct in situ measurements of aerosol particle size help us address this hypothesis and provide additional useful data. We discuss these measurements in more detail in section 4.

[7] Finally, we compare the model results to data from multiple ground-based lidar stations. We use measurements of aerosol optical depth and particle size, where available, from an elastic backscattering lidar in Hefei, China (31.9°N, 117.1°E); two multiwavelength aerosol Raman lidars in Leipzig, Germany (51.4°N, 12.4°E), and Ny-Ålesund, Svalbard (78.9°N, 11.9°E); a lidar in Halifax, Nova Scotia, Canada (44.6°N, 63.6°W), at Dalhousie University; and a lidar at the Mauna Loa Observatory (19.5°N, 155.6°W). More description of these various instruments can be found in section 5. The locations of all of these data sources are shown in Figure 2.

[8] Optical depth comparison will certainly be affected by the model's low spatial resolution, limiting confidence in the model's predictions of local values. This will unlikely significantly impact comparison with the OSIRIS retrievals, as was seen in the study by *Kravitz et al.* [2010], but the point value comparisons, such as with the in situ observations and the lidar retrievals, could potentially be strongly affected. However, because the general circulation of the atmosphere will distribute the aerosols so they are well mixed zonally, the order of magnitude of optical depth should match between the model and these point measurements. We can

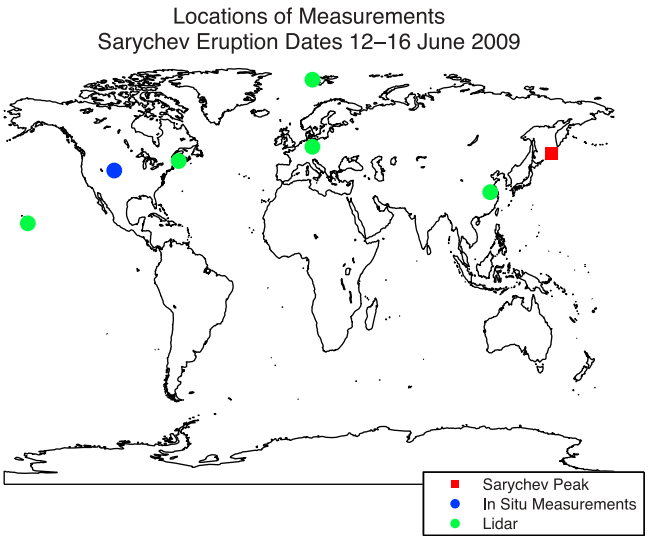

Figure 2. The locations of all point measurements used in our discussion of the Sarychev eruption. The site of the eruption is indicated by a red square. The in situ measurements from Laramie are indicated by a blue dot. Lidar stations are indicated by green dots. OSIRIS is a global measurement, so it cannot be included in this figure.

also use these data sources to perform additional assessments, such as comparisons of atmospheric lifetime and stratospheric removal rates.

[9] The primary purpose of this paper is to explore the differences between modeled sulfate aerosol optical depth and observed optical depth from the Sarychev eruption to analyze possible sources of discrepancy between the two, highlighting potential areas in which the model can be improved. A secondary purpose is to document the Sarychev eruption with an extensive set of observations. We also want to continue the process of comparison of the model results to the OSIRIS retrievals that was begun by *Kravitz et al.* [2010], further showing indispensability of the OSIRIS measurements as a global atmospheric data source.

2. Climate Model

[10] To complete the climate modeling aspect of this study, we simulated the climate response with a coupled atmosphere-ocean general circulation model. We used ModelE, which was developed by the NASA Goddard Institute for Space Studies [*Schmidt et al.*, 2006]. We used the stratospheric version with 4° latitude by 5° longitude horizontal resolution and 23 vertical levels up to 80 km. It is fully coupled to a 4° latitude by 5° longitude dynamic ocean with 13 vertical levels [*Russell et al.*, 1995]. The aerosol module [*Koch et al.*, 2006] accounts for SO_2 conversion to sulfate aerosols, and the radiative forcing (also called "adjusted forcing" by *Hansen et al.* [2005], which is the standard definition of radiative forcing as adopted by the *Intergovernmental Panel on Climate Change* (*IPCC*) [2001]) of the aerosols is fully interactive with the circulation. The dry aerosol radius is specified to be 0.25 μm, and the model hydrates these to form a distribution with a median radius of approximately 0.30–0.35 μm, where aerosol growth is prescribed by formulas used by *Tang* [1996]. This distribution is consistent with the findings of *Stothers* [1997] and was also used in the simulations of the eruptions of Katmai [*Oman et al.*, 2005] and Kasatochi [*Kravitz et al.*, 2010]. For more details on the specifications used in these simulations, see *Kravitz et al.* [2010], which used the same modeling conditions.

[11] Our control ensemble consisted of a 20-member collection of 4 year runs (2007–2010), which involved increasing greenhouse gas concentrations in accordance with the Intergovernmental Panel on Climate Change's A1B scenario [*IPCC*, 2007]. No temperature trend resulting from model spin-up was detected, because of corrective efforts utilizing previously run initial conditions and sufficient tuning.

[12] To examine the effects of the volcanic eruptions, we used a 20-member ensemble of 4 year simulations covering the same time period. In these runs, greenhouse gas concentrations increased in the same manner as in the control runs. We also injected 1.5 Tg of SO_2 into the grid box centered at 52°N, 172.5°W, distributed equally in the three model layers that cover an altitude of 10–16 km, on 12 June 2008. We recognize that the coordinates, amount, and year used in this modeling study are not the same as the actual eruption. We chose these particular values for ease of comparison of our model results with the eruption of Kasatochi volcano on 8 August 2008 in two other studies [*Kravitz et al.*, 2010; *Kravitz and Robock*, 2011]. However, these model simulations are also applicable to this study. Because of the distribution of the sulfate aerosols by the general circulation of the atmosphere, our choice of spatial coordinates in simulating the eruption will not affect the results. Also, the difference in atmospheric composition in the model between the years 2008 and 2009 is negligible, and any differences in results would be due to noise. We have adjusted the labeling in our figures to make the eruption appear as if we simulated it in 2009, and for the reasons we discuss here, this will not be detrimental to our conclusions. According to *Haywood et al.* [2010], the results of which appeared after we completed our model runs, the simulations reflect an incorrect choice of the amount of SO_2 that was injected into the lower stratosphere. We address this later when we discuss the discrepancy between our modeled results and the observations of aerosol optical depth.

[13] ModelE has been shown to be realistic in simulating past volcanic eruptions. Simulations of the climate response to volcanic eruptions with this model have been conducted for the eruptions of Laki in 1783–1784 [*Oman et al.*, 2006a, 2006b], Katmai in 1912 [*Oman et al.*, 2005], and Pinatubo in 1991 [*Robock et al.*, 2007]. In all of these cases, ModelE simulations agreed with observations and proxy records to such a degree that we are confident in this model's ability to predict the climatic impact of volcanic eruptions, meaning model representation of aerosol optical depth is accurate. *Kravitz et al.* [2010] also found the temporal and spatial patterns of optical depth generated by ModelE to be consistent with those measured by OSIRIS.

3. Aerosol Optical Depth: Model Versus OSIRIS

[14] *Kravitz et al.* [2010] performed an extensive comparison between the modeled sulfate aerosol optical depth

and the retrievals obtained by OSIRIS. They encountered a discrepancy of an order of magnitude, some of which was attributed to various assumptions made in both the model and the retrieval of aerosol properties by the satellite instrument. The eruption of Sarychev gives us another opportunity to further investigate this discrepancy.

[15] Figures 3 and 4 show the model calculations of the anomaly in the spatial and temporal extent of total sulfate aerosol optical depth (midvisible, $\lambda = 550$ nm). Anomaly is defined as the difference between the volcano ensemble and the control ensemble, thus removing the contribution to optical thickness from tropospheric sulfate aerosols. Therefore, we refer to these plots as volcanic sulfate aerosol optical depth. The largest anomaly of nearly 0.1 in Figure 3 occurs in August after the eruption. The *e*-folding conversion times for aerosols from the 1982 eruption of El Chichón and the 1991 eruption of Mt. Pinatubo were 30–40 days [*Heath et al.*, 1983; *Bluth et al.*, 1992, 1997; *Read et al.*, 1993], which is the same as given by the more general calculations of *McKeen et al.* [1984]. *Carslaw and Kärcher* [2006] also calculate an *e*-folding time of the chemical conversion rate to be 30 days. The actual conversion rate depends on details specific to each eruption, but this peak anomaly in August is consistent with these reported values of chemical lifetime.

[16] The bulk of the aerosol cloud does not pass south of 30°N, which is consistent with *Stothers* [1996], although smaller values of sulfate optical depth are detectable in the Northern Hemisphere tropics. Large-scale subsidence has removed most of the volcanic aerosols by February after the eruption, with nearly all remnants disappearing before April. Radiative forcing due to the sulfate aerosols becomes smaller in magnitude than -0.25 W m^{-2} well before this time, dropping below this threshold even before winter.

[17] Vertical profiles of stratospheric aerosol extinction were retrieved from the OSIRIS measurements at a wavelength of 750 nm using the SASKTRAN forward model [*Bourassa et al.*, 2008b]. Figure 5 shows a comparison between OSIRIS retrievals and climate model results, divided into three latitude bins. In all latitude bins, background levels are very similar between the model average and OSIRIS, with differences in τ (scaled for wavelength, see below) within ±0.002. The OSIRIS background levels are slightly higher in the Arctic bin (70°–80°N), possibly due to assumptions made in model levels of sulfate aerosols, or perhaps the model has a slightly higher stratospheric removal rate than is found in the atmosphere, resulting in a lower equilibrium level of background aerosol. We discuss later removal rates from the eruption in more detail. The model average is higher in June in the middle bin (50°–60°N) than the OSIRIS retrievals because the model output is given in monthly averages, and by late June, some of the aerosols due to Sarychev would already have formed.

[18] In the middle bin, peak optical depth occurs in July, approximately the same time in both the model and OSIRIS retrievals. Table 1 shows the comparison of decay in optical depth. The *e*-folding lifetimes given are quite low but consistent with the eruption of Kasatochi the previous year [*Kravitz et al.*, 2010]. The model tends to have autumn stratospheric removal rates that are higher than are measured by OSIRIS, based on an exponential fit of the data in Figure 5. However, in the Arctic bin, peak optical depth occurs much later for the model, and in the near-tropical bin (20°–30°N), the peak occurs earlier. This is unlikely due to an incorrect conversion time from SO_2 to sulfate, as a similar problem would be noticeable in all three bins. A likely candidate is improperly calculated stratospheric circulation in the model, which distributes the aerosols to the tropics slightly too quickly and to high latitudes too slowly. However, we are unable to accurately diagnose the cause of this problem at this time.

[19] Similar to the comparison of modeled and retrieved aerosol optical depth for Kasatochi by *Kravitz et al.* [2010], the peak optical depth calculated by ModelE is nearly one full order of magnitude larger than the retrievals obtained from OSIRIS in the Arctic bin and approximately 5 times larger in the middle bin. In the study by Kravitz et al., several possible sources of discrepancy were outlined. One prominent source is the difference in wavelength used to calculate optical depth. ModelE calculates optical depth in the midvisible ($\lambda = 550$ nm), and OSIRIS retrieves in the near-infrared ($\lambda = 750$ nm). Since the radiative effects of the stratospheric aerosols follow an Ångstrom relationship, we would expect this to affect our results.

[20] In ModelE, we assumed an aerosol dry radius of 0.25 μm, which gives an effective radius that is consistent with past data from early 20th century high-latitude volcanic eruptions as found by *Stothers* [1997]. We used this value for the current set of simulations, and it was also used in the simulations of Kasatochi [*Kravitz et al.*, 2010] and Katmai [*Oman et al.*, 2005]. Based on ambient relative humidity values, aerosols of this initial size will increase in radius by, at most, 20%–40%, according to formulas by *Tang* [1996]. These formulas are explicitly used in ModelE and are thus suitable for our calculations. This results in a hydrated aerosol median radius of 0.30–0.35 μm.

[21] Direct calculations using the radiation code offline suggest that scaling of the ModelE results by wavelength to match the OSIRIS retrievals could result in the relation

$$\frac{\text{AOD at 750 nm and } r_{\text{dry}} = 0.25\ \mu\text{m}}{\text{AOD at 550 nm and } r_{\text{dry}} = 0.25\ \mu\text{m}} \approx 0.79. \qquad (1)$$

[22] This corresponds to an Ångstrom exponent of approximately 0.8. *Schuster et al.* [2006] and *Eck et al.* [1999] have measured Ångstrom exponents of this value to be consistent with the particle sizes that we have assumed in our simulations.

[23] This alone does not fully explain the discrepancy between ModelE results and OSIRIS retrievals. One additional source of error could be in assumed particle size. To properly calculate optical depth, the model requires an assumption of particle size. Moreover, the model assumes a unimodal gamma distribution, whereas reality may not have such a clearly defined distribution. *Haywood et al.* [2010]

Figure 3. Time progression of anomaly in stratospheric sulfate aerosol midvisible optical depth for the eruption of Sarychev from June 2009 to February 2010. Both the volcano ensemble and the baseline ensemble are averages of 20 runs. By February 2010, volcanic aerosols remaining in the atmosphere are at very low levels.

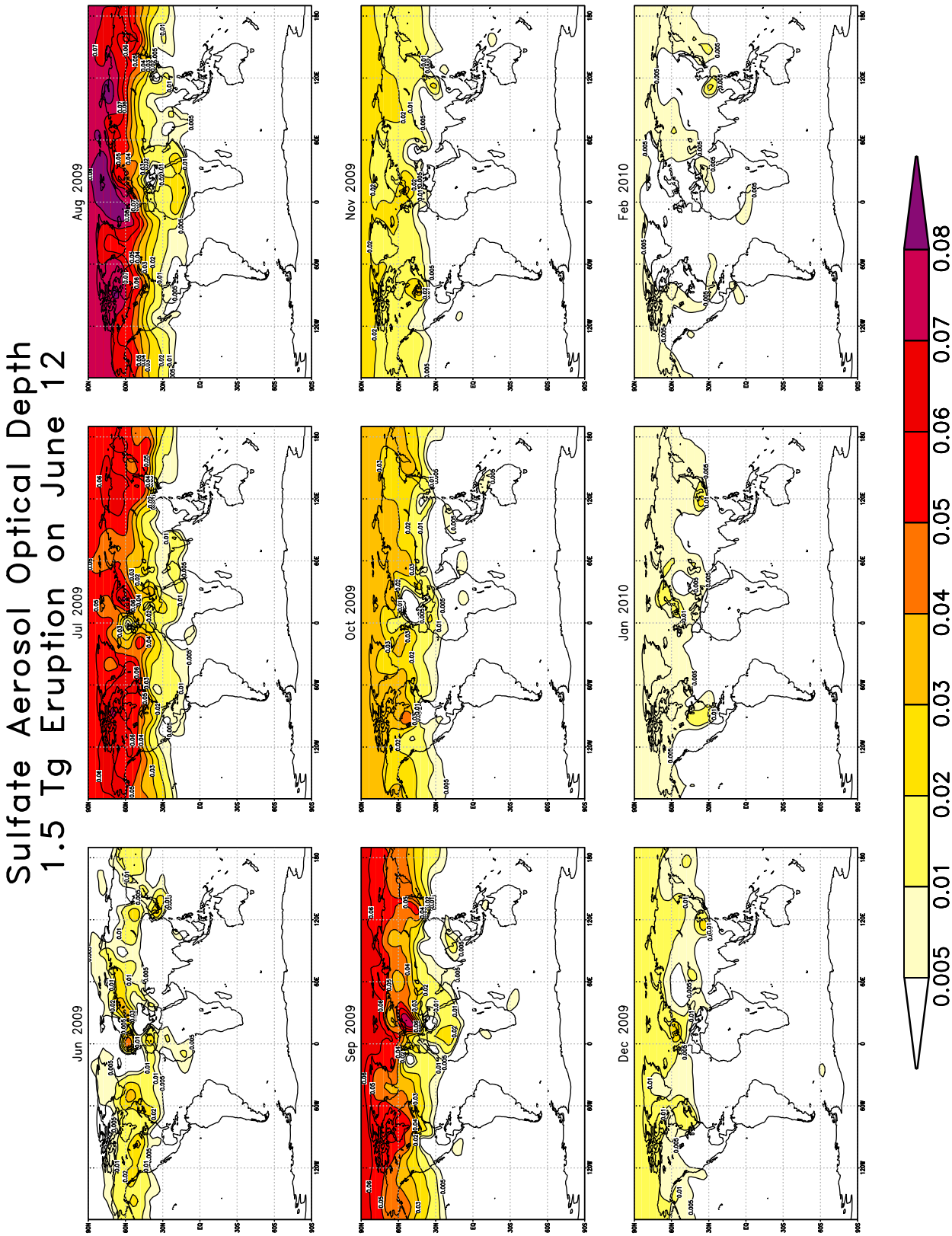
Sulfate Aerosol Optical Depth
1.5 Tg Eruption on June 12
Jun 2009
Jul 2009
Aug 2009
Sep 2009
Oct 2009
Nov 2009
Dec 2009
Jan 2010
Feb 2010
0.005
0.01
0.02
0.03
0.04
0.05
0.06
0.07
0.08

Figure 3

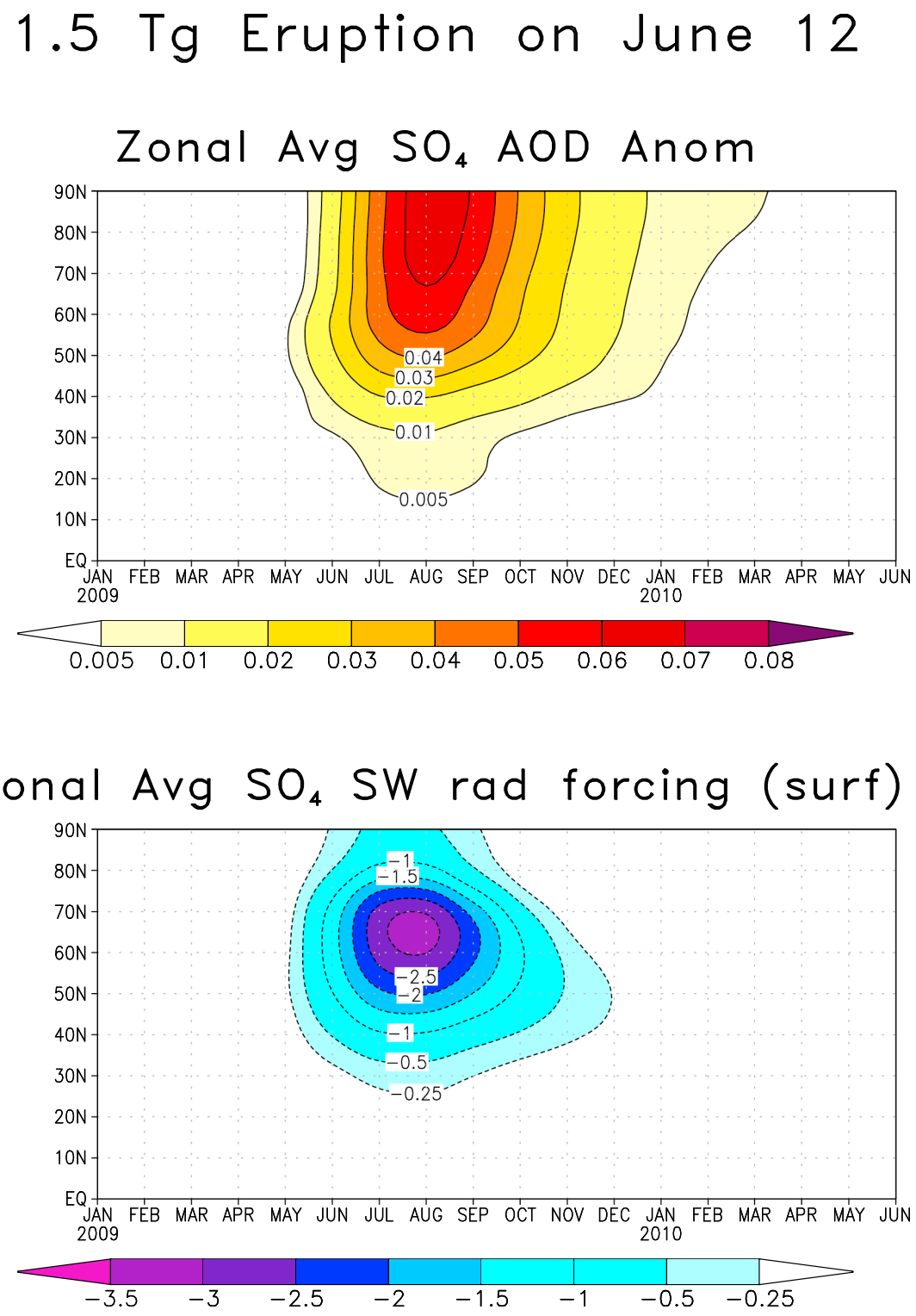

Figure 4. Zonally averaged anomalies in stratospheric sulfate aerosol midvisible optical depth and clear sky shortwave radiative forcing (W m^{-2}) at the surface due to sulfate aerosols. Only the Northern Hemisphere values are plotted, as the Southern Hemisphere values are zero. Results shown are for model simulations of the Sarychev volcanic eruption. Both the volcano ensemble and the baseline ensembles are averages of 20 runs. Results shown here are similar to those in Figure 3, i.e., most of the sulfate aerosols have been deposited out of the atmosphere by February 2010. Radiative forcing due to the sulfate aerosols ceases to be detectable even sooner.

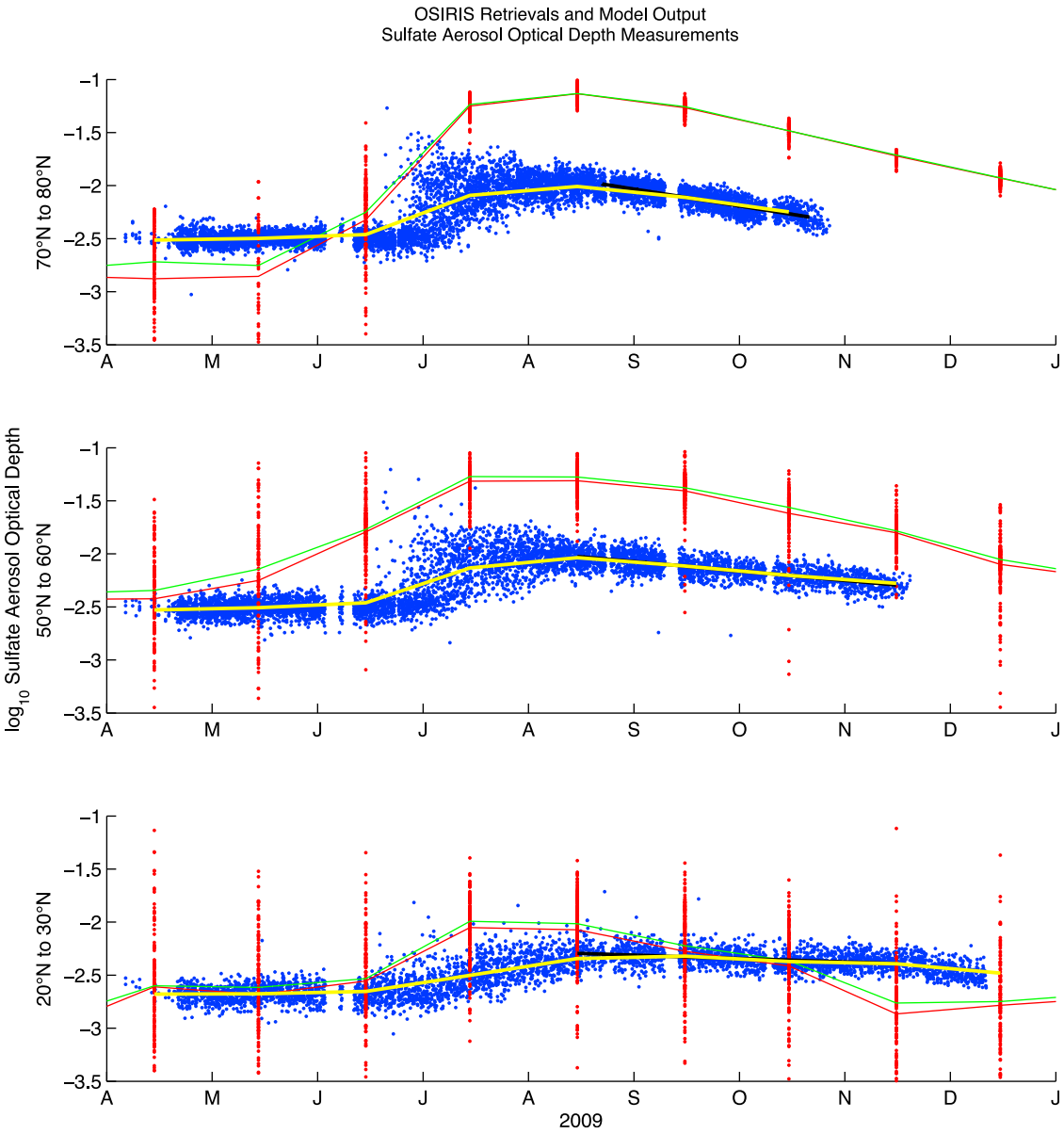

Figure 5. Total stratospheric aerosol optical depth measured by OSIRIS at 750 nm and model results of optical depth at 550 nm. The month labels indicate the beginning of each month. All blue values are individual retrievals from OSIRIS, divided into three latitude bands. Yellow lines are monthly averages of the OSIRIS data, placed on the 15th of each month. All red dots are individual grid box measurements of aerosol optical depth for each latitude band (72 for each latitude that falls into the above bands). The model output is placed on the 15th of each month, as these values represent monthly averages. The red line is an average of all red points ($\log_{10}$ is taken after averaging), indicating an average of model optical depth in the given latitude band. The green line is the median of all red points. Black lines are linear fits to aid in understanding atmospheric deposition rates, the details of which are in Table 1. For OSIRIS measurements, the vertical column extends only from the 380 K level of potential temperature to 40 km altitude. OSIRIS coverage of the Arctic is not available from November to March because of the lack of sunlight.

indeed found two aerosol modes in a lognormal distribution: an Aitken mode with effective radius 0.0065 μm and an accumulation mode of effective radius 0.095 μm. ModelE cannot model aerosols with a dry radius below 0.01 μm, so our model results are incapable of capturing this smaller mode, although due to the very small size of these particles, contributions to optical depth from the Aitken mode are likely not significant. However, even in the accumulation mode, the results of Haywood et al. suggest a gross overestimation of particle size in our modeling study.

[24] We did not have the computing resources to entirely redo our simulations with the correct, smaller aerosol size.

Table 1. Results From the Exponential Fit to Optical Depth Data Shown in Figure 5[a]

Bin	Decay Rate Calculated From Figure 5 ($\log_{10}(\tau)a^{-1}$)	R^2	*e*-Folding Lifetime (Months)
OSIRIS			
70°N–80°N	1.9003	0.59	2.7
50°N–60°N	1.0607	0.50	4.9
20°N–30°N	0.3833	0.10	13.6
ModelE[b]			
70°N–80°N	2.6730	>0.99	1.9
50°N–60°N	2.7113	0.99	1.9
20°N–30°N	2.3871	0.81	2.2

[a]The annual decay rate of optical depth in the model is approximately 5–7 times the decay rate measured by OSIRIS. The *e*-folding lifetime is calculated by the formula 0.4343/*D*, where *D* is the value given in the second column. This formula is obtained from a standard exponential decay equation.
[b]Fit not plotted.

However, we did perform offline calculations using the model's radiation code and specifying a smaller initial aerosol radius. Using this code, the model recalculates the aerosol size distribution, hydrating the aerosols based on the formulas of *Tang* [1996], as well as the scattering efficiencies for these different radii, producing an appropriate Ångstrom relationship for that particle size based on the given SO_2 mass and ambient humidity values. This is not a fully interactive process, in that circulation-dependent results, including transport of the aerosols once they are formed, the spatial distribution of the aerosols throughout their lifetime, and size-dependent deposition rates are not accounted for by this recalculation. Therefore, our presentation of this scaling should be interpreted as if the aerosols were smaller in terms of radiation-dependent effects but not in terms of circulation-dependent effects. However, because of the small size of the particles, in addition to the fact that very little volcanic aerosol was left in the stratosphere by the following spring, such differences are likely minor or negligible. The general spatial patterns, including distributions across different latitude bands, are likely the same for these smaller aerosols as they are for the larger ones.

[25] Using ModelE's radiation code, we specified a dry radius of 0.07 μm, which is less than one third our initial estimate of dry radius. This results in a hydrated aerosol radius of approximately 0.08–0.10 μm. We chose this radius to match the balloon-borne measurements of aerosol median radius, which are discussed in section 4. This much smaller radius results in the relations

$$\frac{\text{AOD at 750 nm and } r_{\text{dry}} = 0.07\ \mu\text{m}}{\text{AOD at 550 nm and } r_{\text{dry}} = 0.25\ \mu\text{m}} \approx 0.43 \tag{2}$$

and

$$\frac{\text{AOD at 750 nm and } r_{\text{dry}} = 0.07\ \mu\text{m}}{\text{AOD at 550 nm and } r_{\text{dry}} = 0.07\ \mu\text{m}} \approx 0.30. \tag{3}$$

[26] The quantity on the right gives an Ångstrom exponent of approximately 3.8, which is quite large but not unreasonable for such small particles [*Eck et al.*, 1999; Schuster *et al.*, 2006]. From this and the quantity given above, we can isolate the effects of reducing the aerosol size, giving us

$$\frac{\text{AOD at 550 nm and } r_{\text{dry}} = 0.07\ \mu\text{m}}{\text{AOD at 550 nm and } r_{\text{dry}} = 0.25\ \mu\text{m}} \approx 1.43 \tag{4}$$

and

$$\frac{\text{AOD at 750 nm and } r_{\text{dry}} = 0.07\ \mu\text{m}}{\text{AOD at 750 nm and } r_{\text{dry}} = 0.25\ \mu\text{m}} \approx 0.54. \tag{5}$$

[27] Optical depth is calculated from the product of number density, extinction, and particle surface area, where extinction increases for smaller particles but decreases with wavelength. These calculations show the complex trade-offs between wavelength and particle size in the context of this experiment, as well as the resulting scaling factors for optical depth.

[28] To some degree, particle size can also have a systematic impact on the OSIRIS results. To retrieve the aerosol extinction profile from limb scatter measurements, the shape of the scattering phase function must be known or assumed. For the OSIRIS retrievals, Mie code is used to calculate the scattering phase function for a lognormal particle size distribution. In this case, the OSIRIS retrievals are performed using the scattering phase function for a median, or mode, radius of 0.08 μm and a mode width of 1.6. Using the above definition, these values correspond to an effective radius of 0.14 μm. These are the same assumptions used for the OSIRIS retrievals of aerosol extinction following the Kasatochi eruption shown by *Kravitz et al.* [2010] and *Bourassa et al.* [2010]. As discussed in detail by *Bourassa et al.* [2007], uncertainty in the particle size distribution systematically affects the retrieved extinction. *McLinden et al.* [1999] showed that for larger particle sizes, most likely in volcanically modified conditions, the phase function remains relatively stable at 750 nm, and systematic error remains on the order a few percent. However, for dramatically larger particle sizes, the impact on the OSIRIS retrievals could be as large as 30% or 40%, adding an additional factor of uncertainty due to particle size in the comparison between OSIRIS and the modeled optical depths.

[29] Another reason explored by *Kravitz et al.* [2010] is the lower altitude level used to calculate the stratospheric aerosol optical depths from the OSIRIS-retrieved extinction profiles. The lower bound is chosen to be the θ = 380 K level of potential temperature. This assumption is made to avoid attempting to retrieve extinction from clouds, dust, and other scattered signal that are not stratospheric sulfate. However, using this as the lower bound for measurements has the potential to reduce optical depth measurements, as OSIRIS will not account for aerosols between the θ = 380 K line and the true thermal tropopause. Figure 6, again, shows optical depth, taking into account this new lower bound, as well as combining the effects of the Ångstrom exponent described above. Compared with Figure 4, optical depth in the midlatitudes and subtropics is largely unchanged, with some areas of slight increase, indicating the thermal tropopause is actually higher than the θ = 380 K line. However, high-latitude optical depth patterns are much lower, sometimes by more than a factor of 2, indicating OSIRIS possibly underestimates high-latitude optical depth by assuming too

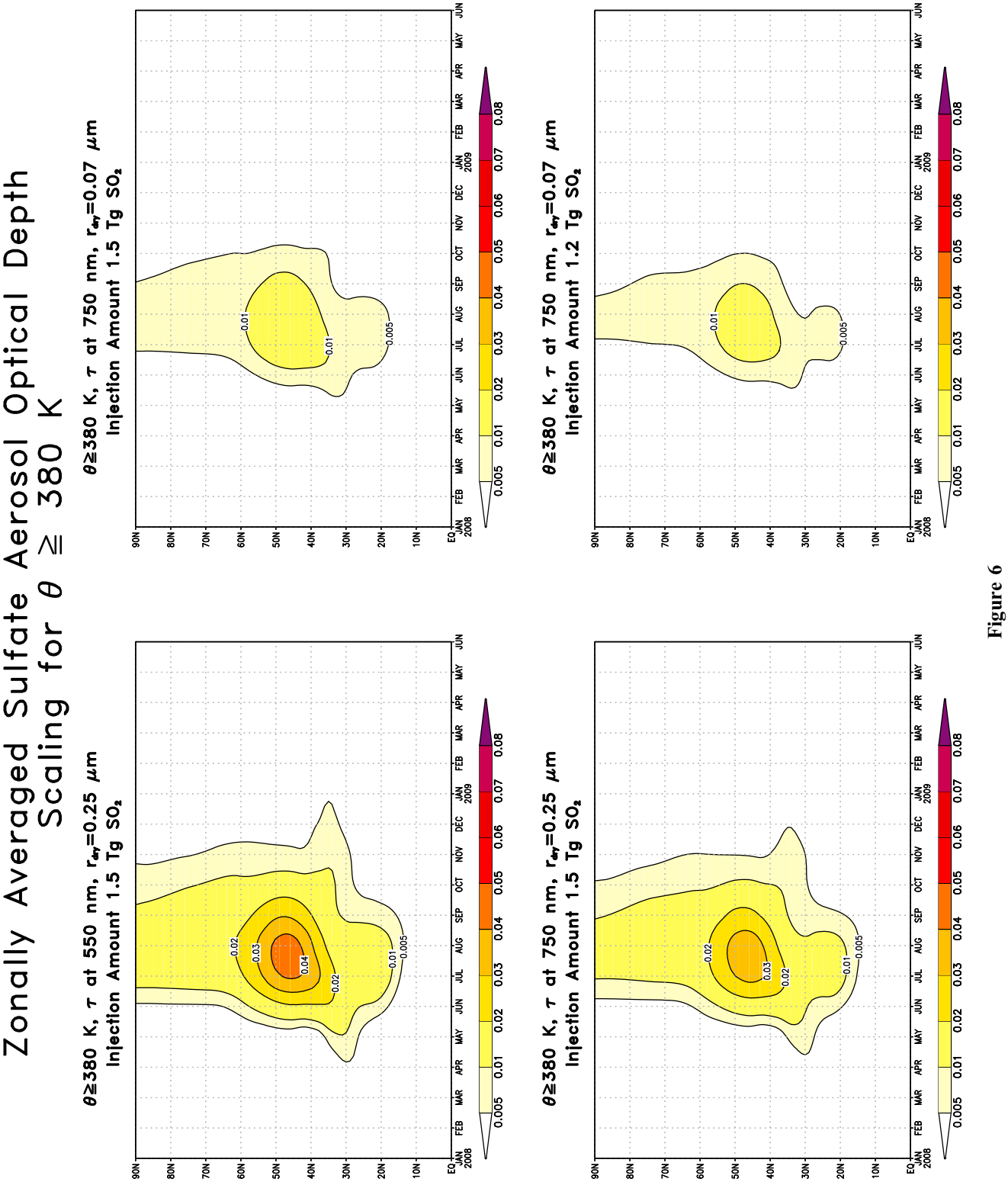
Zonally Averaged Sulfate Aerosol Optical Depth
Scaling for θ ≧ 380 K
θ≧380 K, τ at 550 nm, r_ev=0.25 μm
Injection Amount 1.5 Tg SO2
θ≧380 K, τ at 750 nm, r_ev=0.25 μm
Injection Amount 1.5 Tg SO2
θ≧380 K, τ at 750 nm, r_ev=0.07 μm
Injection Amount 1.5 Tg SO2
θ≧380 K, τ at 750 nm, r_ev=0.07 μm
Injection Amount 1.2 Tg SO2
90N
80N
70N
60N
50N
40N
30N
20N
10N
EQ
JAN 2008
FEB
MAR
APR
MAY
JUN
JUL
AUG
SEP
OCT
NOV
DEC
JAN 2009
FEB
MAR
APR
MAY
JUN
0.005
0.01
0.02
0.03
0.04
0.05
0.06
0.07
0.08

Figure 6

high a base altitude for measurement. Combining these results with scaling due to wavelength, as well as the possibility of using an incorrect aerosol radius, gives Figure 6 (bottom left and top right).

[30] *Haywood et al.* [2010] reported the upper tropospheric/lower stratospheric loading due to Sarychev to be 1.2 Tg of SO_2. Although we were unable to obtain other firm estimations for this value, this indicates our modeled aerosol optical depth values are overestimated by approximately 25%. Arlin Krueger (personal communication, 2010) estimated the atmospheric loading to be 1.5 Tg, which was exactly his estimate of the loading due to Kasatochi. Kai Yang's group at NASA Goddard Earth Sciences and Technology Center reported the atmospheric loading to be near 2.0 Tg SO_2 (A. Krueger, personal communication), which was the same value they reported for the eruption of Kasatochi [*Yang et al.*, 2010]. Since the model results show higher optical depths than the OSIRIS retrievals, we suspect the model overestimated the atmospheric loading. For the purposes of calculating discrepancy, we will assume we overestimated the atmospheric loading in our model calculations, so we scale our model results by 0.8 (1.2 divided by 1.5). The results of this are shown in Figure 6 (bottom right). Figure 6 (bottom right) shows that the maximum overestimation of aerosol optical depth by the model due to these reasons is quite large, although not as large as the overestimation of optical depth due to Kasatochi in the study by *Kravitz et al.* [2010].

[31] Figure 7 shows the combination of these three sources of error in comparison with OSIRIS retrievals. When these potential errors are taken into account, the fit of the model to the observations of the volcanic aerosols is quite good. Under this scaling, the fit to the background level of stratospheric aerosols is very poor, which is expected, since the assumptions we made regarding overestimation are specific to volcanic aerosols. Also, the mismatch of aerosol decay rates between the model and observations becomes visibly clear. The decay rate in the summer appears to be good, but the autumn decay rate in the model appears to be larger than is observed. Also more apparent is the peak in optical depth in the 20°–30°N latitude band, which is larger and earlier in the model than in observations.

[32] *Kravitz et al.* [2010] discovered evidence for additional sources of discrepancy in their comparison, some of which may also be relevant to the eruption of Sarychev. Although we cannot quantify the degree to which they might affect our results, we can briefly discuss them.

[33] One of the largest potential sources of discrepancy is that not all of the SO_2 may have been injected above the tropopause, meaning some of the aerosols would have formed in the troposphere and deposited very rapidly. This leaves the option that the model's overestimation of SO_2 loading is even greater than is discussed above.

[34] Additionally, as was found by *Schmale et al.* [2010] for the eruption of Kasatochi, not all of the volcanic aerosol layer is necessarily composed of sulfate, which will affect the radiative properties of the aerosol layer. Schmale et al. also discovered some SO_2 remained as late as 3 months after the eruption, possibly indicating overly rapid conversion of SO_2 into sulfate in the model. However, this is not unreasonable, as an *e*-folding lifetime of 1 month would mean approximately 5% of the SO_2 should still remain after this time. Both of these reasons could indicate a potential source of additional overestimation of sulfate aerosol optical depth by the model, although we do not have enough information to quantify them as they relate to the eruption of Sarychev.

[35] Finally, some additional possible sources of discrepancy are related to possibly inaccurate representations of removal processes in the model. The phase of the quasi-biennial oscillation and its effects on the removal efficiency and the phase and magnitude of tropical modes are unknown, but we would not necessarily expect the model to accurately represent these processes, given the large natural variabilities of these processes.

[36] We note that in Figure 5, with the exception of the 70°–80°N bin, the spread of the modeled values of optical depth is much larger than the spread of OSIRIS retrievals. This cannot be directly attributed to any specific cause, but many of the sources of discrepancy discussed above for average aerosol optical depth could also apply to the model spread. Also, meteorological conditions in the model are different from the real world, which certainly could have an impact on the spread of our results. The spread of the observations could potentially decrease if we reran the model simulations with the correct aerosol size distribution, which would account for changes in magnitude and distribution of optical depth values, but again, we are unable to undertake this prohibitively expensive computational endeavor.

4. Comparison Using in Situ Aerosol Profiles

[37] Our second means of comparison with model output is in situ aerosol measurements from balloon-borne instruments lofted from Laramie, Wyoming (41.3°N, 105.7°W). Use of this very long-term data source has been well established for both volcanic eruptions and background stratospheric aerosol concentrations [e.g., *Deshler et al.*, 2006]. The size resolved number concentration measurements are fit to either unimodal or bimodal lognormal size distributions of the form [e.g., *Hofmann and Deshler*, 1991; *Deshler et al.*, 1993]

$$n(r) = \sum_{i=1}^{2} \frac{N_i}{\ln(\sigma_i)\sqrt{2\pi}} \cdot \frac{1}{r} \exp\left[-\frac{\ln^2(r/r_i)}{2 \cdot \ln^2(\sigma_i)}\right], \qquad (6)$$

where N_i is aerosol number density, r_i is the aerosol median radius, and σ_i is the standard deviation of the distribution.

Figure 6. Zonally averaged total stratospheric aerosol optical depth anomaly as calculated by the model. (top left) Anomaly in zonally averaged optical depth, scaled using the θ = 380 K line as the tropopause instead of the thermal tropopause. (bottom left) The same field multiplied by 0.79 to reflect the difference in measured optical depth due to a change in wavelength, assuming a dry radius of 0.25 μm. (top right) Scaled using the θ = 380 K line as the tropopause and also multiplied by 0.43 to reflect the difference in measured optical depth due to a change in wavelength, assuming a dry radius of 0.07 μm. (bottom right) The same as at top right but multiplied by 0.8 to reflect our overestimation of the initial SO_2 loading, which should have been 1.2 Tg instead of 1.5 Tg.

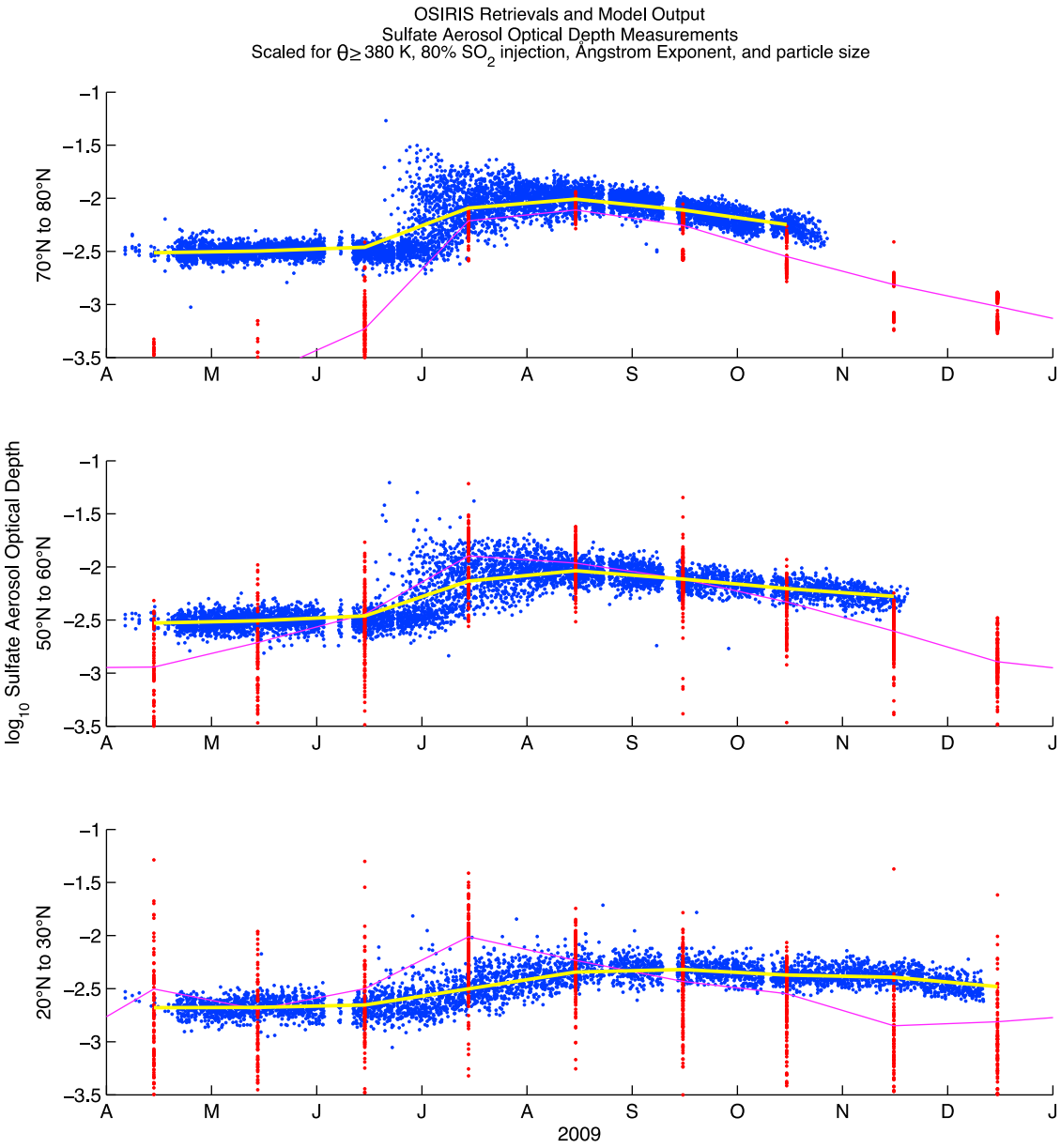

Figure 7. OSIRIS retrievals and model output of sulfate aerosol optical depth, as in Figure 5, but scaled to reflect sources of discrepancy. OSIRIS retrievals (blue) and means (yellow) are unchanged from the values in Figure 5. Model output is scaled using the θ = 380 K line as the tropopause instead of the thermal tropopause, multiplied by 0.8 to reflect our overestimation of the initial SO_2 loading, which should have been 1.2 Tg instead of 1.5 Tg, and multiplied by 0.43 to reflect a scaling to 750 nm (for comparability with OSIRIS) and as an estimate of the inaccuracy in our choice of particle size, as discussed in section 3. All multiplication is performed before taking $\log_{10}$. Red dots are individual model output points, as in Figure 5, and the magenta line is their average.

Deshler et al. [2003] provided more details on the specifics of the measurements, their uncertainties, and the derivation of size distributions and their moments. Measurement uncertainties lead to an error of the fits by ±30% for the median radius, ±20% for the standard deviation, and ±40% for surface area and volume. In the aerosol measurements following the Sarychev eruption, the larger aerosol mode has such a low number concentration that the fit is effectively unimodal. *Deshler et al.* [1997] showed the Pinatubo aerosols developed a clearly bimodal structure approximately 40 days after the eruption, so perhaps the Sarychev eruption did not eject enough material to create this larger mode.

[38] Figure 8 shows in situ measurements from 22 June 2009, 10 days after the initial eruption of Sarychev. For comparison, it also shows results from 3 July 2007, over 1 year after Soufriere Hills and prior to Kasatochi. This 2007 sounding was chosen because it was approximately the

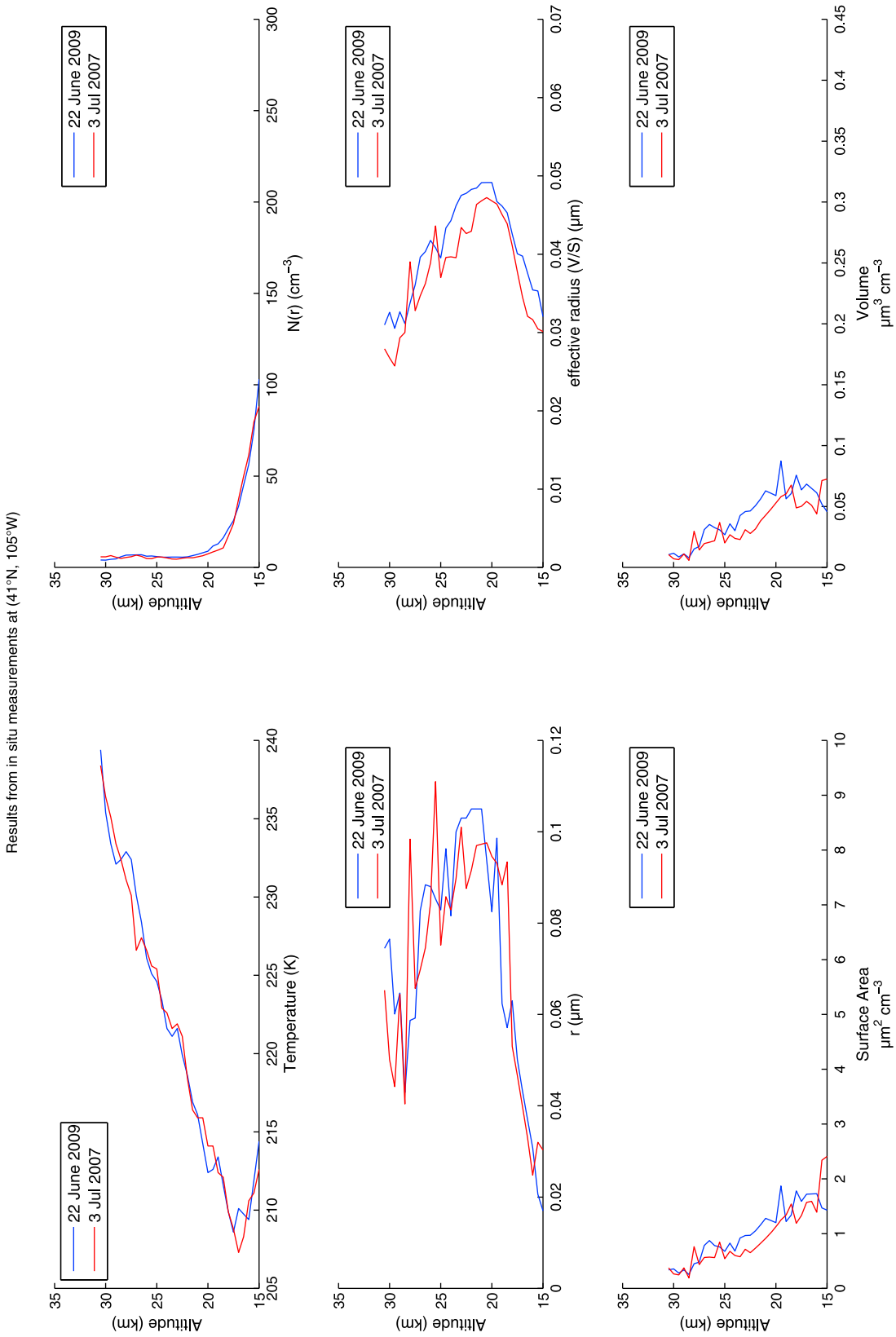

Figure 8. Profiles of temperature, total aerosol concentration (condensation nuclei), aerosol median radius, effective radius, surface area, and volume derived from size resolved particle concentration measurements from balloon flights from Laramie, Wyoming. Temperature and number concentration are measured, and the other products are derived. The blue line shows measurements on 22 June 2009, 10 days after the largest eruption of Sarychev. The red line shows 3 July 2007, which was free of volcanic activity after Soufriere Hills in 2006 and prior to Kasatochi. Measurements are shown from the 22 June 2009 tropopause at 15.0 km to balloon burst at 30.5 km.

same time of year as the 22 June 2009 sounding, has a similar temperature profile, and was a relatively clean period for volcanic eruptions. We chose a sounding within close temporal proximity to 2009, as the stratospheric aerosol layer has become increasingly thick since approximately 2000, so only recent soundings would be suitable for comparison [*Hofmann et al.*, 2009].

[39] The 2009 measurements show no significant differences from the 2007 measurements. If the chemical lifetime of SO_2 for this eruption is on the lower end of the estimates given in the previous section, then a measurable amount of aerosols from Sarychev would have been formed by 22 June 2009. Given an *e*-folding lifetime of 1 month for the conversion of SO_2 to sulfate, approximately 28% of the aerosol mass would have been converted by this time. Moreover, back trajectory calculations show the volcanic plume could have reached Laramie by this time [*Haywood et al.*, 2010].

[40] Radiosondes are launched every 12 h from Sakhalin Island (47.0°N, 142.7°E), which is very close to the eruption site of Sarychev (48.1°N, 153.2°E). The initial plume height of 11–16 km [*Haywood et al.*, 2010] corresponds to a potential temperature range of 342–400 K, according to radiosonde data from 00Z 16 June 2009 [*Durre et al.*, 2006]. This station is southwest of the eruption site, so this result should not have been altered by the eruption, because of the predominating westerlies at this latitude. Because of the stratosphere's inherent stability, stratospheric motion is often confined to isentropic layers [*Holton*, 2004]. Although cross-isentropic motion is possible because of diabatic heating or lofting of the isentropes due to the pressure wave of the volcanic eruption, it is plausible that the volcanic plume remained confined to this range of potential temperatures through its passage over Laramie. The 22 June 2009 sounding reports the potential temperature range of 342–400 K corresponds to an altitude range from below the tropopause up to 16 km. Therefore, it is unlikely that the measurements from 22 June 2009 show any aerosols from the Sarychev eruption, as these altitudes show little difference from background levels.

[41] Figure 9, similar to Figure 8, shows results from measurements on 7 November 2009, 5 months after the eruption, and on 17 October 2005. The 2005 measurements were chosen because 2005 was a quiescent year for stratospheric aerosols, yet according to *Hofmann et al.* [2009] was still close enough in time to the eruption to have comparable levels of background stratospheric aerosol, and the time of year and tropopause heights were similar in both profiles. The aerosols have had time to be created and age since the June sounding, resulting in much larger volumes and surface areas. The aerosols have also settled, which is evidenced by a large area of increased volume and surface area from the tropopause (13.0 km at this time and latitude) to 19.0 km in altitude, with a strong peak at 14.0 km. The reported median radius at 14 km in altitude is approximately 0.07–0.08 μm, which motivates our choice of radius in the calculations in section 3. We note that the in situ measurements show an effective radius peak of 0.06 μm, more than 2 times smaller than the calculated effective radius of 0.14 μm used in the OSIRIS calculations. This could also have an impact on our results, although as was seen in section 3, the complex calculations involved in optical depth do not allow us to quantify the potential effects on our comparison.

[42] The results from an in situ measurement taken in the following March (data not shown) show no significant stratospheric aerosol features. *Deshler et al.* [1997] calculated a subsidence rate in the Southern Hemisphere of 3–4 km a^{-1} for the stratospheric aerosols from Pinatubo, which is consistent with the fall rate of a particle of radius 0.5 μm. This radius is much larger than the Sarychev aerosols, implying that gravitational settling mechanisms would result in a much slower fall speed for the Sarychev aerosols. However, assuming the Pinatubo settling rate for the eruption of Sarychev, the aerosol plume would have descended no more than 1.5–2 km over the period June to November and 2.5–3 km over the period June to March. Therefore, to explain the large peaks in Figure 9 at 14.0 km, the initial plume height cannot have been greater than 16.0 km in altitude. This is again consistent with the results of *Haywood et al.* [2010]. However, if the initial plume height were 16.0 km, at the same settling rate, the aerosols could not have descended below 13.0 km by March 2010. The tropopause height in March was measured to be 11.0 km, and no significant stratospheric aerosol layers were detected at this time in the model results or any of the data sources, meaning all aerosols had fallen out of the stratosphere and thus must have descended lower than this height. Thus, assuming a rate of gravitational settling identical to the Pinatubo rate is contrary to our findings, meaning it is likely that the Sarychev aerosols had a higher settling rate than the Pinatubo aerosols.

[43] This faster settling rate can be explained by a number of factors. A large part of the atmospheric lifetime of stratospheric aerosols is due to poleward transport, where large-scale descent of air in the winter is responsible for removal of the aerosols [e.g., *Hamill et al.*, 1997]. If the aerosols already begin at high latitudes, as in the case of Sarychev, the absence of the need for poleward transport will necessarily decrease the atmospheric lifetime. *Oman et al.* [2005] obtained similar results in their simulations, as they found an *e*-folding lifetime of 1 year for aerosols from Pinatubo, a tropical eruption, and 8–9 months for aerosols from Katmai, a high-latitude eruption. Moreover, a large part of the aerosol plume from Sarychev is concentrated in the midlatitude storm tracks, where tropopause folding is responsible for removal of stratospheric aerosols [e.g., *Kravitz et al.*, 2009]. Finally, the amount of aerosols in the stratosphere was not large enough for a significant portion to resist the large-scale mechanisms involved in stratospheric removal of the aerosols, meaning very little aerosol remained in the stratosphere by the following spring. Conversely, Pinatubo was a very large eruption, injecting gases and particles to much higher altitudes, and thus aerosols remained in the stratosphere for multiple years afterward. The processes controlling stratospheric aerosol removal at higher altitudes may be weighted quite differently than processes near the tropopause, where dynamics plays a more important role. These differences may account for the calculation of a slower gravitational settling rate from Pinatubo [*Deshler et al.*, 1997].

[44] Mie theory was used to calculate aerosol extinction profiles and optical depth at 758 nm from the in situ aerosol profiles on 17 October 2005, 22 June 2009, and 7 November 2009 (Figure 10). The profiles and optical depths on 17 October 2005 and 22 June 2009 are quite

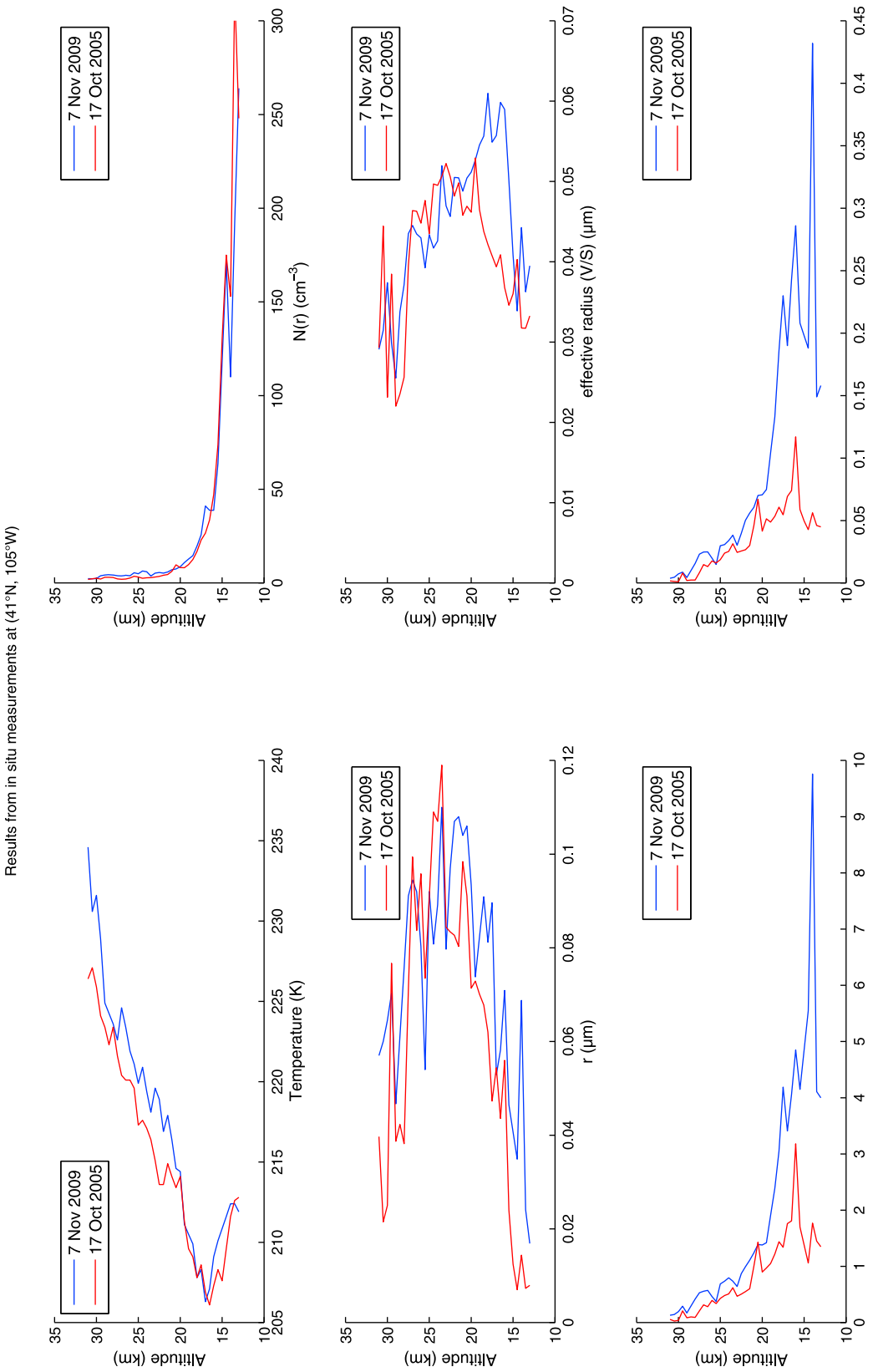

Figure 9. Same as Figure 8 but for measurements from Laramie, Wyoming, on 7 Nov 2009 (blue line), several months after the eruption of Sarychev, and 17 Oct 2005 (red line), which was a period of low perturbations of stratospheric aerosol with otherwise similar atmospheric conditions to the 2009 measurement. Measurements are shown from the tropopause, at 13.0 km, to balloon burst at 31.0 km. The volcanic layer appears to have begun to settle through the lower stratosphere, with a large peak at 14.0 km in altitude.

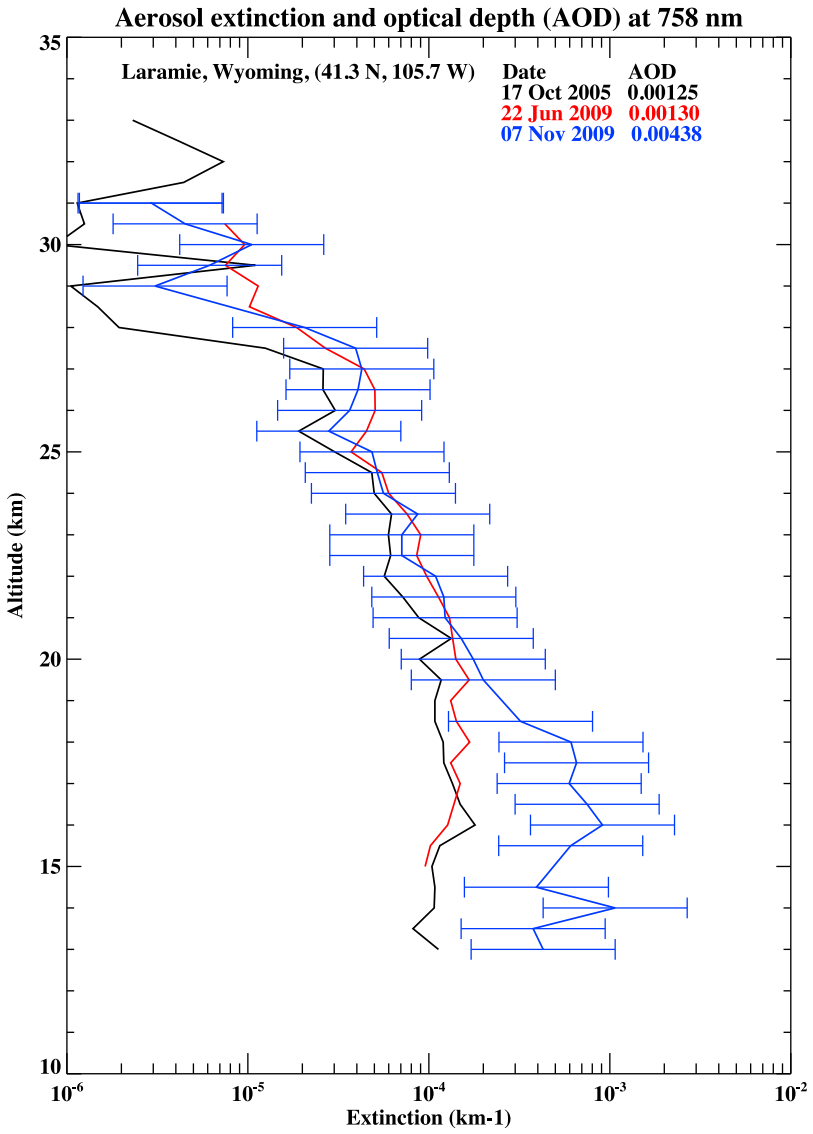

Figure 10. Aerosol extinction profiles from in situ measurements on 17 October 2005, 22 June 2009, and 7 November 2009, calculated at 758 nm. The lower limits of the lines are defined by the tropopause on each day. The error bars on 7 November 2009 represent a ±40% uncertainty and apply to the other two profiles as well. The aerosol optical depth (AOD) for each day is shown at the top.

similar. In contrast, the 7 November 2009 sounding shows a stratospheric optical depth of 0.0044, over 3 times higher than observed earlier. The increase in optical depth on 7 November 2009 is from an increase in aerosol between the tropopause and 20 km, which is due to the eruption of Sarychev. The first column of Table 2 shows a comparison between monthly mean values of the in situ measurements, model calculations, and OSIRIS retrievals. Model values are scaled to account for the relevant sources of discrepancy discussed in section 3, including changes in optical depth due to wavelength. For November 2009, which is the month for which all three of these sources have volcanic aerosol values, the agreement between all three sources is quite good. The largest difference is between an optical depth of 0.0044 (in situ) and 0.0033 (OSIRIS), a difference of 25% of the in situ measurements, which is well within the threshold of measurement error.

5. Further Comparison Using Lidar Data

[45] To better characterize our results, our simulations will be compared with observations from five ground-based lidar sources in Hefei, China (31.9°N, 117.1°E); Leipzig, Germany (51.4°N, 12.4°E); Ny-Ålesund, Svalbard (78.9°N, 11.9°E); Halifax, Nova Scotia, Canada (44.6°N, 63.6°W); and Mauna Loa, Hawaii (19.5°N, 155.6°W) (Figure 2).

[46] The lidar measurements were all performed at 532 nm, which is close to the 550 nm wavelength used to calculate the model results, so no scaling for wavelength is required. However, to account for an overestimation of atmospheric loading of SO_2, the model results are multiplied by 0.8.

Table 2. Comparison of Optical Depth Between the Model OSIRIS and the in Situ and Lidar Measurements From June Through December 2009[a]

Month	Averages	Laramie	Hefei (50 sr)	Leipzig (38 sr)	Svalbard (50 sr)	Halifax (40 sr)	Mauna Loa (40 sr)
Jun	Observations	0.0013	0.0015	0.0039	0.0072	0.0001	N/A
	Model	0.0024	0.0006	0.0042	0.0018	0.0032	0.0001
	Model σ	0.0213	0.0139	0.0241	0.0078	0.0220	0.0075
	OSIRIS	N/A	N/A	N/A	N/A	N/A	0.0025
Jul	Observations	N/A	0.0022	0.0090	0.0135	0.0031	0.0006
	Model	0.0110	0.0031	0.0161	0.0192	0.0134	0.0022
	Model σ	0.0190	0.0118	0.0258	0.0114	0.0210	0.0102
	OSIRIS	N/A	N/A	N/A	N/A	N/A	0.0025
Aug	Observations	N/A	0.0032	0.0095	0.0108	0.0023	0.0009
	Model	0.0075	0.0040	0.0149	0.0256	0.0115	0.0029
	Model σ	0.0170	0.0096	0.0231	0.094	0.0200	0.0099
	OSIRIS	0.0010	0.0029	0.0009	0.0011	0.0010	0.0026
Sep	Observations	N/A	0.0038	0.0072	0.0108	0.0012	0.0009
	Model	0.0071	0.0015	0.0123	0.0197	0.0098	0.0017
	Model σ	0.0199	0.0169	0.0211	0.0075	0.0184	0.0073
	OSIRIS	0.0039	0.0034	0.0038	0.0047	0.0039	0.0030
Oct	Observations	N/A	0.0030	0.0078	N/A	N/A	0.0008
	Model	0.0037	0.0013	0.0078	0.0121	0.0059	0.0008
	Model σ	0.0176	0.0153	0.0189	0.0036	0.0180	0.0048
	OSIRIS	0.0037	0.0034	0.0038	0.0023	0.0037	0.0030
Nov	Observations	0.0044	0.0023	0.0055	N/A	0.0001	0.0007
	Model	0.0037	0.0006	0.0050	0.0068	0.0042	0.0001
	Model σ	0.0115	0.0172	0.0109	0.0021	0.0118	0.0051
	OSIRIS	0.0033	0.0032	0.0035	0.0024	0.0033	0.0032
Dec	Observations	N/A	0.0020	0.0054	N/A	0.0001	0.0005
	Model	0.0020	0.0008	0.0027	0.0042	0.0027	0.0000
	Model σ	0.0072	0.0167	0.0067	0.0016	0.0066	0.0073
	OSIRIS	N/A	N/A	N/A	N/A	N/A	N/A

[a]All values given are monthly averages and are at 750 nm in wavelength. The lidar ratio for each source is given in parentheses. In each column, the top value is the observation (scaled), the second value is the model (scaled), and the third value is OSIRIS (unscaled). The Laramie optical depth measurements are calculated at 758 nm, so no scaling is required. The Leipzig lidar already includes data scaled to 750 nm in wavelength (Figure 13). All other lidar data are measured at 532 nm and are thus multiplied by 0.30, as described in section 3. Model output is for the 4° latitude band (zonal average) containing the site of the point measurement. Model values are first multiplied by 0.8 to reflect an overestimation of SO_2 loading and then by 0.43 to scale the values to 750 nm, as described in section 3. OSIRIS values are for the 5° latitude band (zonal average) containing the point observation. All values are rounded to four decimal places. Any field marked by N/A has no data available for that month.

Additionally, to account for an overestimation of particle size in the model, the model results are multiplied by 1.43, as discussed in section 3. We would also like to include OSIRIS results in our comparison. Since OSIRIS retrievals are at 750 nm, we use the scaling factors in section 3, dividing all OSIRIS retrievals by 0.30 to scale them to 550 nm. In the comparisons in this section, we are unable to properly account for differences between the thermal tropopause and the baseline for OSIRIS measurements (θ = 380 K). In this section, all model and OSIRIS results are zonally averaged. The model's latitudinal resolution is 4°, so all model results are zonal averages over the 4° latitude band containing the observation point. Averaging is similar for OSIRIS, but with a resolution of 5° latitude.

[47] The lidar in Hefei is an elastic backscattering lidar for profiling aerosol backscatter coefficient at 532 nm based on a Nd:YAG laser with a second harmonic generator. Aerosol coefficient profiles below about 25 km above ground level were derived from lidar data using the Fernald method with an assumed lidar ratio of 50 sr.

[48] The results from this lidar (Figure 11) show a peak in backscatter in September 2009 at an altitude of 18–19 km, which corresponds to an aerosol optical depth of approximately 0.014. All profiles are very similar above 21 km in altitude, suggesting this as an upper bound for the plume height. July 2009 shows a slight peak, whereas the profile for June 2009 is nearly identical to months prior. All backscatter profiles from December 2009 onward are similar to the background. However, aerosol optical depth measurements from 2010 are slightly larger than in early 2009, prior to the eruption, suggesting a small amount of aerosol remained in the stratosphere through at least the winter following the eruption.

[49] The aerosol optical depth measurements at Hefei are qualitatively similar to the model results. Both show optical depths of similar magnitudes, although a peak optical depth of approximately 0.014 occurs 1 month earlier in the model than in observations. This reiterates the problem shown in section 3, again possibly indicating too rapid transport of the modeled aerosols to the tropics. We also see a much more rapid decay of stratospheric aerosol optical depth in the model, reaching background levels nearly immediately after the peak values. OSIRIS retrievals show peak optical depth at the same time as the lidar, although the peak is lower and the decay rate is much less pronounced. Table 2 reiterates this comparison in more detail. The altitude of reported peak backscatter is at a similar altitude to peak aerosol retrievals in the 7 November 2009 in situ measurements.

[50] MARTHA (Multiwavelength Atmospheric Raman lidar for Temperature, Humidity, and Aerosol profiling), a multiwavelength Raman lidar in Leipzig, Germany, has been in operation since 1996 [*Mattis et al.*, 2010]. From it, we can obtain vertical profiles of the particle backscatter coefficient at the three wavelengths of 355, 532, and 1064 nm;

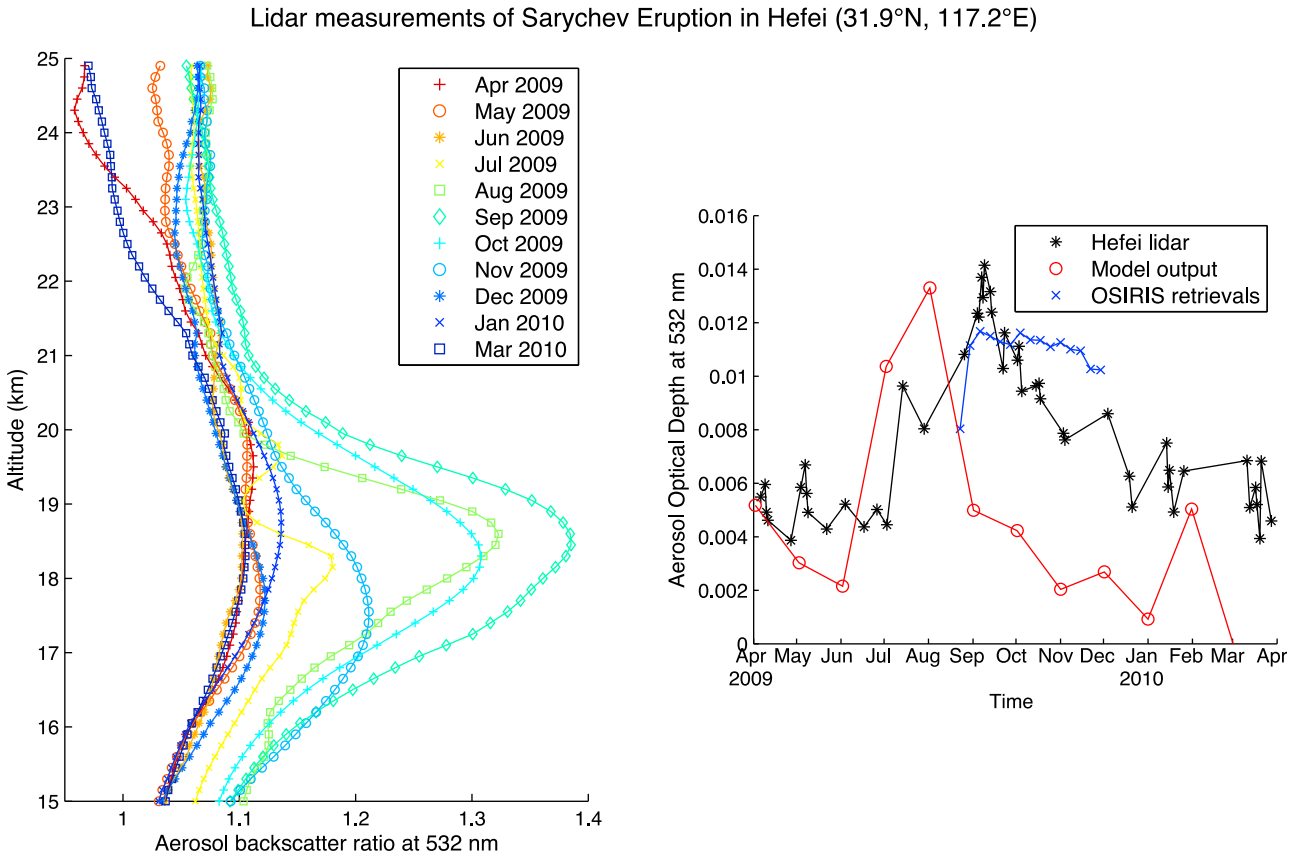

Figure 11. Lidar retrievals from Hefei, China compared with ModelE output and OSIRIS retrievals. The lidar is capable of measuring backscatter up to 25 km in altitude. (left) Monthly averages of backscatter as a function of altitude, with a maximum in September 2009. The backscatter ratio is defined as the fraction $\frac{\beta_{\text{molecules}}+\beta_{\text{particles}}}{\beta_{\text{molecules}}}$, where β is backscatter, so any values less than 1 are spurious and are likely due to instrument noise. (right) The black line shows integrated (15–25 km) optical depth (532 nm) through the stratosphere, assuming a lidar ratio of 50 sr. The red line shows zonally averaged stratospheric aerosol optical depth (550 nm) calculated by the model in the grid latitude band containing the Hefei lidar (28°–32°N), multiplied by 0.8 to reflect an overestimation of SO_2 loading from the eruption and by 1.43 to reflect an overestimation of particle radius (as discussed in section 3). The blue line shows OSIRIS retrievals (750 nm), zonally averaged over the latitude band 30°–35°N, divided by 0.30 to account for differences in wavelength. Aerosol concentrations return to background levels by spring of the year following the eruption.

the extinction coefficient at 355 and 532 nm; the corresponding lidar ratio at 355 and 532 nm; and profiles of the depolarization ratio at 532 nm. *Mattis et al.* [2002a, 2002b] and *Ansmann et al.* [2002] described in more detail the current system in operation, as well as error analysis. This lidar has been used to evaluate the aerosol cloud resulting from past volcanic eruptions, including Pinatubo [*Mattis*, 1996; *Ansmann et al.*, 1997] and Kasatochi [*Mattis et al.*, 2010]. It has also had success in retrieving aerosol microphysical properties [*Wandinger et al.*, 1995; *Müller et al.*, 1999].

[51] The results from this lidar (Figure 12) show optical depth measurements about a factor of 2 lower than model results. The peak value of approximately 0.025 occurs in late July and mid-August, which is 2–4 weeks later than modeled peak optical depth of approximately 0.05 (scaled to resolve discrepancy). Table 2 compares some of the values in more detail. This factor of 2 can be explained by several potential reasons. The spatial distribution of the volcanic plume in the model would not be expected to perfectly match the lidar observations, especially considering the coarse spatial resolution of the model. Also, several assumptions in both the model and observations could alter the results, including the assumed lidar ratio of approximately 38 in determining optical depth, the base altitude from which backscatter is integrated, and inaccurate corrective scaling that was discussed in section 3. We are unable to accurately quantify the degree to which our comparison is affected by these unknown factors. Aerosol optical depth returns to near-background levels by December following the eruption.

[52] To partly resolve discrepancies between this lidar and OSIRIS, Figure 13 shows the same backscatter results as Figure 12, but optical depth is recalculated at 750 nm, using both the thermal tropopause and the 380 K potential temperature line as the lower bound for integration. The OSIRIS retrievals in September, October, and November appear to match the adjusted lidar retrievals quite well, as do the background measurements taken in June. However, the

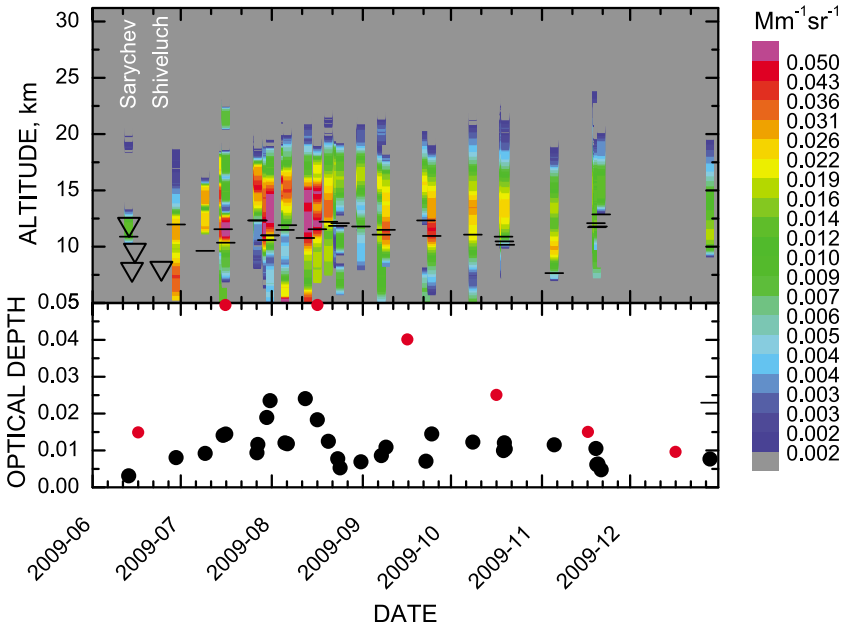

Figure 12. Backscatter coefficient profiles at 1064 nm and aerosol optical depth at 532 nm from the lidar in Leipzig. Backscatter coefficients are defined as the scattering coefficient (units m^{-1}) at 180° (units sr^{-1}) and are scaled by 10^{-6}, giving units of Mm^{-1} sr^{-1}. Each strip of backscatter measurements is a 10 day mean profile. Aerosol optical depth was calculated using a lidar ratio of 38 sr, which is the mean value of all cases for which the lidar ratio could be measured. Black dots are stratospheric optical depth measurements calculated using this ratio. Red dots show zonally averaged stratospheric aerosol optical depth calculated by the model in the grid latitude band containing the Leipzig lidar (48°–52°N), multiplied by 0.8 to reflect an overestimation of SO_2 loading from the eruption and by 1.43 to reflect an overestimation of particle radius (as discussed in section 3). Black horizontal lines indicate the height of the tropopause. Triangles show the plume top heights of individual eruptive events. Peak-measured backscatter and optical depth occur in mid-August, and aerosols have returned to low levels by winter following the eruption.

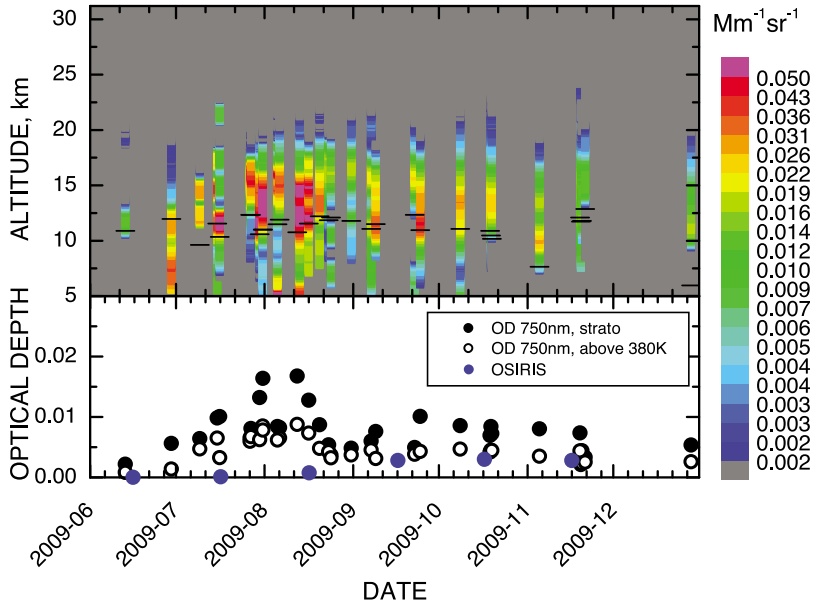

Figure 13. Same as Figure 12, but optical depth is recalculated at 750 nm, using both the thermal tropopause and the 380 K potential temperature line as the lower bound for integration. OSIRIS retrievals (750 nm), zonally averaged over the latitude band 50°–55°N, are shown in blue.

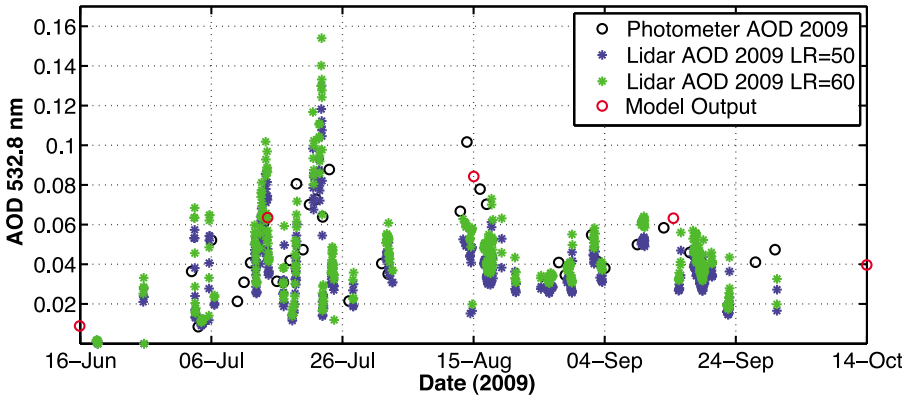

Figure 14. Aerosol optical depth at 532 nm from the KARL lidar and an SP1A Sun photometer in Ny-Ålesund, Svalbard. Lidar aerosol optical depth was calculated using two different lidar ratios of 50 and 60 sr and integrating the extinction coefficient between the thermal tropopause height and 20 km. The lidar ratios were obtained in case studies from 13 July (50 ± 10 sr) and 3 September (60 ± 10 sr) according to the transmittance method [*Chen et al.*, 2002]. The tropopause height was derived from colocated daily balloon soundings. Photometer aerosol optical depth (AOD) are daily means, which are reduced by the monthly long-term means from 1995 to 2008 without extreme events (June, 0.07; July, 0.05; August, 0.045; September, 0.035). Model output is zonally averaged stratospheric aerosol optical depth (550 nm) in the grid latitude band containing the Svalbard lidar (76°–80°N), multiplied by 0.8 to reflect an overestimation of SO_2 loading from the eruption and by 1.43 to reflect an overestimation of particle radius (as discussed in section 3). Model output values represent monthly averages, so they are placed on or near the 15th of each month. OSIRIS retrievals are very small compared to the depicted values, so they are not shown.

match in July and August during peak aerosol loading is rather poor. Table 2 shows a discrepancy in those months of several orders of magnitude, whereas the modeled results compare quite well with the observations.

[53] The Koldewey Aerosol Raman Lidar (KARL) is part of the Alfred Wegener Institute for Polar and Marine Research and Polar Institute Paul Emile Victor (AWIPEV) research base in Ny-Ålesund, Svalbard (78.9°N, 11.9°W; www.awipev.eu), and has been in operation since 2001. The light source is a Nd:YAG laser, which transmits pulses at the three wavelengths of 355, 532, and 1064 nm at a repetition rate of 50 Hz. With a 70 cm telescope, elastic backscattering at those three wavelengths as well as N_2 and H_2O Raman signals and the depolarization ratio at the two shorter wavelengths are detected. Backscatter coefficient profiles are calculated using the Klett method with different lidar ratios [*Klett*, 1981]. KARL has mainly been used for characterizing the Arctic spring troposphere, where Arctic haze occurs [*Ritter et al.*, 2004; *Hoffmann et al.*, 2009]. In recent years, stratospheric volcanic aerosols, e.g., from the Kasatochi volcano [*Hoffmann et al.*, 2010], have also been observed.

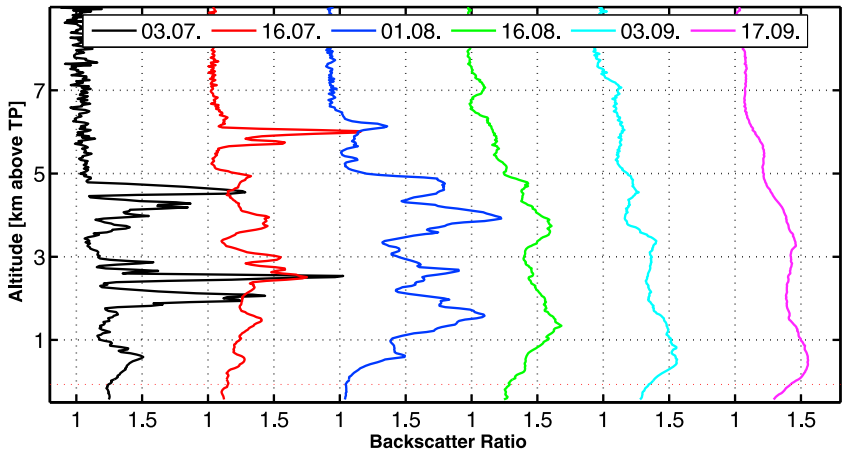

Figure 15. Backscatter ratio profiles at 532 nm for selected days (30 min temporal and 30 m spatial resolutions) for the KARL lidar in Ny-Ålesund, Svalbard. Altitude is scaled relative to the thermal tropopause height, which is obtained from colocated daily balloon soundings. In the first 2 months after the eruption, distinct layers with maximum backscatter ratio above 2 are measured. Late August and September show much smoother profiles with still large values of up to 1.5.

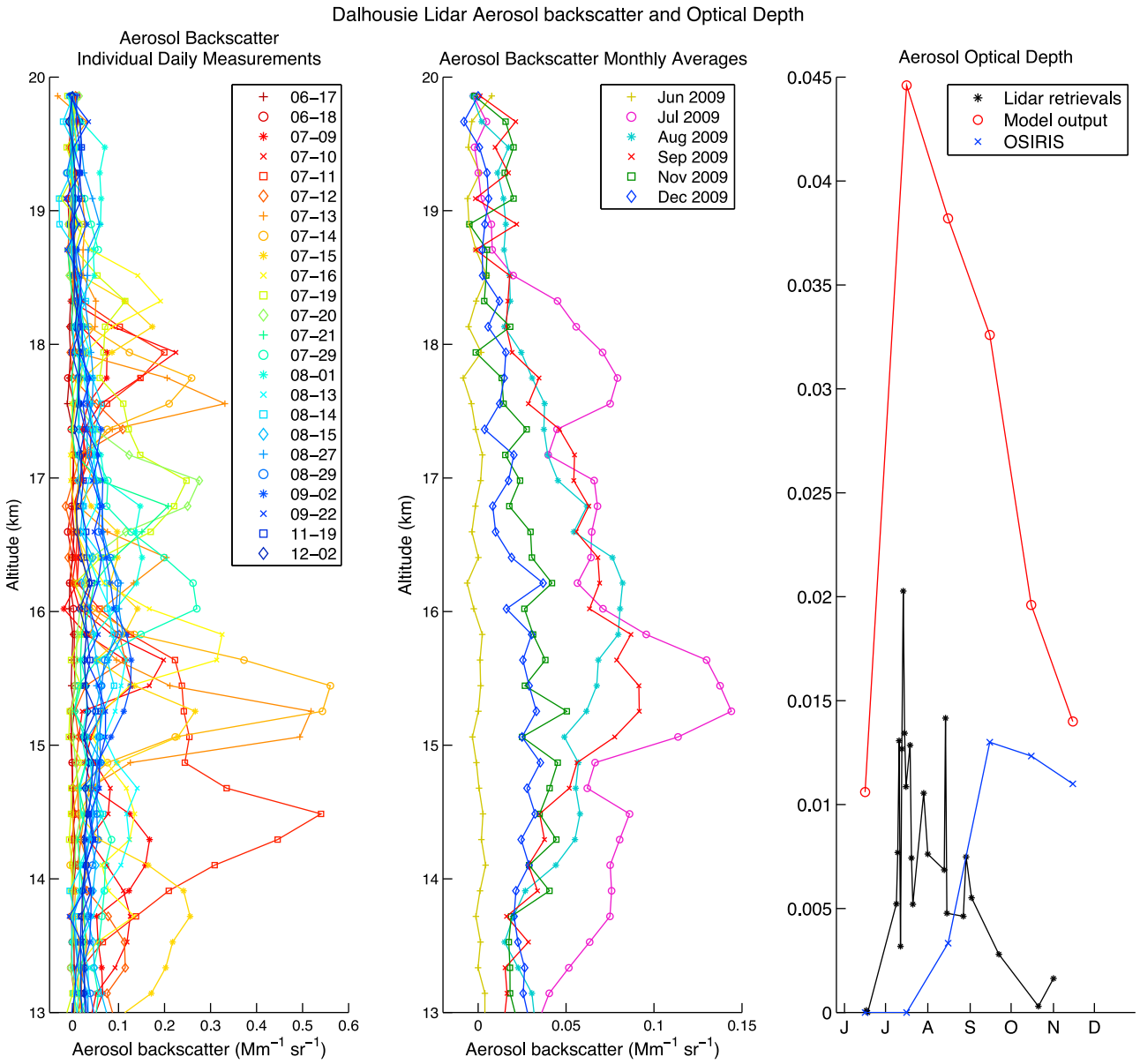

Figure 16. Backscatter and aerosol optical depth from the lidar in Halifax. Backscatter is measured at 532 nm, and the units are the same as in Figure 12. Measurements below 13 km in altitude show strong interference from cirrus clouds and are omitted. Aerosol optical depth was calculated using a lidar ratio of 40 sr. Lidar optical depth values are averaged between 15 and 20 km to avoid interference from cirrus clouds. At right, the red line shows zonally averaged stratospheric aerosol optical depth (550 nm) calculated by the model in the grid latitude band containing the Halifax lidar (44°–48°N), multiplied by 0.8 to reflect an overestimation of SO_2 loading from the eruption and by 1.43 to reflect an overestimation of particle radius (as discussed in section 3). The blue line shows OSIRIS retrievals (750 nm), zonally averaged over the latitude band 40°–45°N, divided by 0.30 to account for differences in wavelength.

[54] The results from KARL and the colocated photometer (Figure 14) agree very well with the model simulations, in that modeled optical depth values and decay rates are nearly identical to the lidar retrievals. Table 2 quantifies this in more detail, showing that the comparison between lidar and the model are quite close, with differences in July, August, and September often remaining below a factor of 2. Conversely, OSIRIS performs rather poorly at this latitude, in that most differences from the lidar observations are approximately 1 order of magnitude. Measured peak optical depth occurs in late July, which is earlier than the August peak in the model. This is also consistent with the comparison with OSIRIS, in which modeled optical depth peaked later than measured optical depth at this latitude. The temporal variability of backscatter ratios and hence aerosol optical depth is very high within the first 2 months after the volcanic eruption, due to the occurrence of several distinct layers of enhanced backscatter (Figure 15). The maximum sulfate aerosol optical depth of over 0.12 is found in July above Spitsbergen. In September, stratospheric aerosol

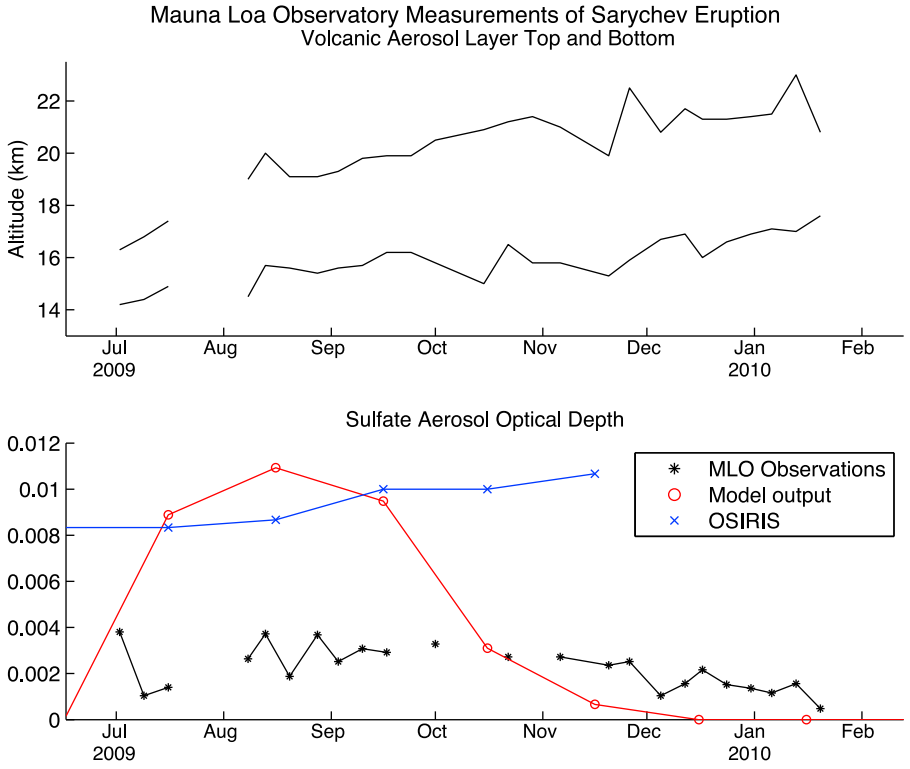

Figure 17. Observations of the Sarychev eruption cloud from the Mauna Loa Observatory (MLO). Some observations are missing because of interference from cirrus clouds. (top) The top and bottom of the Sarychev aerosol layer as measured at the Mauna Loa Observatory. (bottom) The black line shows optical depth calculations from the observatory, which are obtained from measured backscatter using a lidar ratio of 40 sr. The red line shows zonally averaged stratospheric aerosol optical depth (550 nm) calculated by the model in the grid latitude band containing the Mauna Loa lidar (16°–20°N), multiplied by 0.8 to reflect an overestimation of SO_2 loading from the eruption and by 1.43 to reflect an overestimation of particle radius (as discussed in section 3). The blue line shows OSIRIS retrievals (750 nm), zonally averaged over the latitude band 15°–20°N, divided by 0.30 to account for differences in wavelength.

optical depth was still high, with values exceeding 0.05, but less variable, due to a more uniform distribution of the sulfate aerosols within the stratosphere. The temporal evolution of aerosol optical depth shown in Figure 14 matches the model output for the Arctic bin in Figure 5. As stated earlier, these values are much higher than the aerosol optical depths obtained with OSIRIS but could be confirmed by colocated Sun photometer measurements. These values are higher than the in situ measurements by approximately 1 order of magnitude, but the comparability of these two sources of measurement is uncertain, due to the large difference in latitude between the two sites.

[55] The Dalhousie Raman Lidar is operated in Halifax, Nova Scotia, Canada (44.6°N, 63.6°W), and measures vertical profiles of atmospheric scattering. The instrument employs a frequency-doubled ND:YAG laser that transmits pulses of 532 nm wavelength light into the atmosphere at a repetition rate of 20 Hz. The receiver consists of a 25 cm telescope and photomultipliers with fast-counting electronics to detect the signals. Profiles of the aerosol backscatter cross section are derived from the measured elastic lidar signals using the Klett Inversion technique [*Klett*, 1981], assuming a constant lidar ratio of 40 sr for stratospheric aerosols. A more detailed description of the instrument and aerosol optical property retrievals can be found in the study by *Bitar et al.* [2010].

[56] The results for the lidar in Halifax (Figure 16) show peak backscatter in July of very similar values to peak backscatter in the Leipzig lidar results. The altitudes of this peak backscatter are more concentrated, ranging between 14 and 16 km for the Halifax results and 12–16 km for the Leipzig results. Also, the peak occurs approximately 1 month earlier than the Leipzig measurements. These altitude ranges are consistent with model input, the findings of *Haywood et al.* [2010], and the in situ measurements discussed in section 4. Backscatter is near background levels for the June and December measurements. Calculations of optical depth show a peak of approximately 0.02, again in July, with a lower peak in August. This temporal pattern matches the model output quite well, although the modeled values of optical depth are approximately a factor of 2–3 larger than the retrievals. The decay rate of optical depth also matches between the two sources. The in situ measurements in November are approximately 1 order of magnitude higher than the lidar measurements, but we are unable to determine what caused this large discrepancy. The OSIRIS observations do not match the lidar retrievals, showing near-background levels in July and a peak in

September, although the magnitude of this peak is of similar magnitude to the peak optical depth measured by the lidar, which occurs in July.

[57] The NOAA Mauna Loa Observatory lidar uses a 30 Hz Nd:YAG laser producing the 1064 nm and 532 frequency-doubled wavelengths. The power at each wavelength is about 15 W, and two 61-cm-diameter mirrors are used to collect the scattered light. Photon-counting photomultiplier tubes are used for both wavelengths and are electronically gated when needed. The data acquisition electronics has a 300 m altitude resolution, and files are normally saved every 5.6 min. The molecular signal is usually normalized in the interval from 35 to 40 km. The molecular profile is derived from the Hilo radiosonde and a Mass Spectrometer Incoherent Scatter model for the upper stratosphere. The error due to the signal statistics is about 5%. The lidar is a primary instrument of the Network for the Detection of Atmospheric Composition Change.

[58] Figure 17 shows weekly observations from the Mauna Loa Observatory. The lidar detected aerosols from the Sarychev eruption as early as July 1, at which time the aerosol cloud remained confined to 14–16 km in altitude, which is similar to the in situ measurements. Throughout its lifetime, the plume rose in altitude and spread to an altitude of approximately 16–23 km, which is still the lower stratosphere in the tropics. The plume ceased to be detectable by February 2010. Modeled optical depth at this latitude shows a large peak in August of approximately 0.01 (scaled), whereas the lidar shows a rather consistent optical depth, reaching a slight peak of 0.004. Modeled optical depth also decays much more rapidly, showing very low levels by November 2010, whereas the lidar detected aerosols for a few months after. The OSIRIS retrievals (scaled for wavelength) show a more constant temporal evolution in optical depth, similar to the lidar observations, but the OSIRIS measurements are larger by a factor of 2–3. However, our scaling methods are imperfect, so perhaps this discrepancy can be explained, in part, by our choice of scaling factors.

6. Discussion and Conclusions

[59] Evaluating the results in Table 2 more generally, the model does a reasonably good job of reproducing the measurements obtained from the in situ profiles, lidar backscatter, and OSIRIS. It appears to perform much better in the midlatitudes and high latitudes, with sometimes questionable performance in the tropics. However, since optical depths in the tropics are so low for high-latitude eruptions, perhaps model fidelity in the tropics is less important. We see repeated evidence that suggests problems with stratospheric circulation in the model, distributing aerosols to the tropics too quickly and the poles too slowly. All of the observations fall well within the model spread ($\pm 1\sigma$), but the standard deviations of the model results are large.

[60] The results presented have many different sources of error, which we have discussed in detail. Although our corrections for improper simulated aerosol size and atmospheric SO_2 loading, as well as our corrections for wavelength for intercomparability of observations, are all plausible, they undoubtedly introduce some amount of error that we are unable to further quantify. In combination with the inherent sources of error in the observations, it is conceivable that all of the values presented agree to within assumed error.

[61] ModelE tends to have stratospheric aerosol removal rates in the autumn that are higher than observed, which affected the temporal comparison of optical depth. This is likely, in part, due to our overestimation of aerosol size, although when viewed in light of the aforementioned stratospheric circulation issues, this reason probably cannot explain the entire discrepancy.

[62] We reiterate that OSIRIS is an accurate, indispensable means of obtaining stratospheric aerosol optical depth. Not only is it relatively consistent with lidar retrievals and in situ observations, but its global coverage provides data where the other observation methods discussed previously cannot. OSIRIS is an essential part of a volcanic aerosol observation system that needs a great deal of improvement. A range of reported amount of SO_2 injected into the stratosphere, if used to force a climate model, would result in a large range of predicted climate effects. Moreover, estimates of aerosol particle size are very sparse. As we discuss in section 3, accurate measurement of particle size, both initially and as the aerosols age, are essential to accurate determining the radiative effects.

[63] **Acknowledgments.** We thank Arlin Krueger for estimates of SO_2 loading, Jim Haywood for his generous help in providing us with useful measurements on which we based some of our calculations, Mark Miller for helpful discussion of our results, and the reviewers for their comments. We thank Jason Hopper, Kimiko Sakamoto, Stephen Doyle, and Chris Hung for operating the Dalhousie Raman Lidar. The KARL lidar was operated by AWIPEV base personnel Henning Kirk and Marcus Schumacher, and Sun photometer data were provided and processed by Andreas Herber and Maria Stock. Model development and computer time at the Goddard Institute for Space Studies were supported by National Aeronautics and Space Administration climate modeling grants. OSIRIS work was supported in part by the Natural Sciences and Engineering Research Council of Canada and the Canadian Space Agency. Odin is a Swedish-led satellite project funded jointly by Sweden (SNSB), Canada (CSA), France (CNES), and Finland (Tekes). The work of B. Kravitz and A. Robock was supported by NSF grant ATM-0730452. The in situ particle measurements from Laramie were supported by NSF grant ATM-0437406.

References

Ansmann, A., I. Mattis, U. Wandinger, F. Wagner, J. Reichardt, and T. Deshler (1997), Evolution of the Pinatubo aerosol: Raman lidar observations of particle optical depth, effective radius, mass and surface area over Central Europe at 53.4°N, *J. Atmos. Sci.*, *54*, 2630–2641, doi:10.1175/1520-0469(1997)054<2630:EOTPAR>2.0.CO;2.

Ansmann, A., F. Wagner, D. Müller, D. Althausen, A. Herber, W. von Hoyningen-Huene, and U. Wandinger (2002), European pollution outbreaks during ACE 2: Optical particle properties inferred from multiwavelength lidar and star-Sun photometry, *J. Geophys. Res.*, *107*(D15), 4259, doi:10.1029/2001JD001109.

Bitar, L., T. J. Duck, N. I. Kristiansen, A. Stohl, and S. Beauchamp (2010), Lidar observations of Kasatochi volcano aerosols in the troposphere and stratosphere, *J. Geophys. Res.*, *115*, D00L13, doi:10.1029/2009JD013650.

Bluth, G. J. S., S. D. Doiron, A. J. Krueger, L. S. Walter, and C. C. Schnetzer (1992), Global tracking of the SO_2 clouds from the June, 1991 Mount Pinatubo eruptions, *Geophys. Res. Lett.*, *19*, 151–154, doi:10.1029/91GL02792.

Bluth, G. J. S., W. I. Rose, I. E. Sprod, and A. J. Krueger (1997), Stratospheric loading of sulfur from explosive volcanic eruptions, *J. Geol.*, *105*, 671–684, doi:10.1086/515972.

Bourassa, A. E., D. A. Degenstein, R. L. Gattinger, and E. J. Llewellyn (2007), Stratospheric aerosol retrieval with OSIRIS limb scatter measurements, *J. Geophys. Res.*, *112*, D10217, doi:10.1029/2006JD008079.

Bourassa, A. E., D. A. Degenstein, and E. J. Llewellyn (2008a), Retrieval of stratospheric aerosol size information from OSIRIS limb scattered sunlight spectra, *Atmos. Chem. Phys.*, *8*, 6375–6380, doi:10.5194/acp-8-6375-2008.

Bourassa, A. E., D. A. Degenstein, and E. J. Llewellyn (2008b), SASKTRAN: A spherical geometry radiative transfer code for efficient estimation of limb scattered sunlight, *J. Quant. Spectrosc. Radiat. Transfer*, *109*, 52–73, doi:10.1016/j.jqsrt.2007.07.007.

Bourassa, A. E., D. A. Degenstein, B. J. Elash, and E. J. Llewellyn (2010), Evolution of the stratospheric aerosol enhancement following the eruptions of Okmok and Kasatochi: Odin-OSIRIS measurements, *J. Geophys. Res.*, *115*, D00L03, doi:10.1029/2009JD013274.

Budyko, M. I. (1977), *Climatic Changes*, 261 pp., AGU, Washington, D. C.

Carslaw, K. S., and B. Kärcher (2006), Stratospheric aerosol processes, in *Stratospheric Processes and Their Role in Global Climate (SPARC), A Project of WMO/ICSU/IOC World Climate Research Program: Assessment of Stratospheric Aerosol Properties (ASAP)*, *SPARC Rep. 4*, pp. 1–28, SPARC Sci. Steering Group, Univ. of Toronto, Toronto, Onta., Canada, http://www.atmosp.physics.utoronto.ca/SPARC/ASAP%20V3c1.pdf.

Chen, W., C. Chiang, and J. Nee (2002), Lidar ratio and depolarization ratio for cirrus clouds, *Appl. Opt.*, *41*, 6470–6476, doi:10.1364/AO.41.006470.

Deshler, T., B. J. Johnson, and W. R. Rozier (1993), Balloonborne measurements of Pinatubo aerosol during 1991 and 1992 at 41°N, vertical profiles, size distribution, and volatility, *Geophys. Res. Lett.*, *20*, 1435–1438, doi:10.1029/93GL01337.

Deshler, T., J. B. Liley, G. Bodeker, W. A. Matthews, and D. J. Hofmann (1997), Stratospheric aerosol following Pinatubo, comparison of the North and South mid latitudes using in situ measurements, *Adv. Space Res., 20*(11), 2089–2095, doi:10.1016/S0273-1177(97)00600-5.

Deshler, T., M. E. Hervig, D. I. Hofmann, J. M. Rosen, and J. B. Liley (2003), Thirty years of in situ stratospheric aerosol size distribution measurements from Laramie, Wyoming (41°N), using balloon-borne instruments, *J. Geophys. Res.*, *108*(D5), 4167, doi:10.1029/2002JD002514.

Deshler, T., R. Anderson-Sprecher, H. Jäger, J. Barnes, D. J. Hofmann, B. Clemesha, D. Simonich, M. Osborn, R. G. Grainger, and S. Godin-Beekmann (2006), Trends in the nonvolcanic component of stratospheric aerosol over the period 1971–2004, *J. Geophys. Res.*, *111*, D01201, doi:10.1029/2005JD006089.

Durre, I., R. S. Vose, and D. B. Wuertz (2006), Overview of the Integrated Global Radiosonde Archive, *J. Clim.*, *19*(1), 53–68, doi:10.1175/JCLI3594.1.

Eck, T. F., B. N. Holben, J. S. Reid, O. Dubovik, A. Smirnov, N. T. O'Neill, I. Slutsker, and S. Kinne (1999), Wavelength dependence of the optical depth of biomass burning, urban, and desert dust aerosols, *J. Geophys. Res.*, *104*(D24), 31,333–31,349, doi:10.1029/1999JD900923.

Gao, C., L. Oman, A. Robock, and G. L. Stenchikov (2007), Atmospheric volcanic loading derived from bipolar ice cores accounting for the spatial distribution of volcanic deposition, *J. Geophys. Res.*, *112*, D09109, doi:10.1029/2006JD007461.

Hamill, P., E. J. Jensen, P. B. Russell, and J. J. Bauman (1997), The life cycle of stratospheric aerosol particles, *Bull. Am. Meteorol. Soc.*, *78*, 1395–1410, doi:10.1175/1520-0477(1997)078<1395:TLCOSA>2.0.CO;2.

Hansen, J., et al. (2005), Efficacy of climate forcings, *J. Geophys. Res.*, *110*, D18104, doi:10.1029/2005JD005776.

Haywood, J., et al. (2010), Observations of the eruption of the Sarychev volcano and simulations using the HadGEM2 climate model, *J. Geophys. Res.*, *115*, D21212, doi:10.1029/2010JD014447.

Heath, D. F., B. M. Schlesinger, and H. Park (1983), Spectral change in the ultraviolet absorption and scattering properties of the atmosphere associated with the eruption of El Chichón: Stratospheric SO_2 budget and decay, *Eos Trans. AGU*, *64*, 197.

Hoffmann, A., C. Ritter, M. Stock, M. Shiobara, A. Lampert, M. Maturilli, T. Orgis, R. Neuber, and A. Herber (2009), Ground-based lidar measurements from Ny-Ålesund during ASTAR 2007, *Atmos. Chem. Phys.*, *9*, 9059–9081, doi:10.5194/acp-9-9059-2009.

Hoffmann, A., C. Ritter, M. Stock, M. Maturilli, S. Eckhardt, A. Herber, and R. Neuber (2010), Lidar measurements of the Kasatochi aerosol plume in August and September 2008 in Ny-Alesund, Spitsbergen, *J. Geophys. Res.*, *115*, D00L12, doi:10.1029/2009JD013039.

Hofmann, D. J., and T. Deshler (1991), Stratospheric cloud observations during formation of the Antarctic ozone hole in 1989, *J. Geophys. Res.*, *96*, 2897–2912, doi:10.1029/90JD02494.

Hofmann, D., J. Barnes, M. O'Neill, M. Trudeau, and R. Neely (2009), Increase in background stratospheric aerosol observed with lidar at Mauna Loa Observatory and Boulder, Colorado, *Geophys. Res. Lett.*, *36*, L15808, doi:10.1029/2009GL039008.

Holton, J. (2004), *An Introduction to Dynamic Meteorology*, 4th ed., 535 pp., Elsevier, Burlington, Mass.

Intergovernmental Panel on Climate Change (IPCC) (2001), *Climate Change 2001: The Scientific Basis. Contribution of Working Group I to the Third Assessment Report of the Intergovernmental Panel on Climate Change*, edited by J. T. Houghton et al., Cambridge Univ. Press, Cambridge, U. K.

Intergovernmental Panel on Climate Change (IPCC) (2007), *Climate Change 2007: The Physical Science Basis. Contribution of Working Group I to the Fourth Assessment Report of the Intergovernmental Panel on Climate Change*, edited by S. Solomon et al., Cambridge Univ. Press, Cambridge, U. K.

Klett, J. D. (1981), Stable analytical inversion solution for processing lidar returns, Appl. Opt., 20, 211–220, doi:10.1364/AO.20.000211.

Koch, D., G. A. Schmidt, and C. V. Field (2006), Sulfur, sea salt, and radionuclide aerosols in GISS ModelE, *J. Geophys. Res.*, *111*, D06206, doi:10.1029/2004JD005550.

Kravitz, B., and A. Robock (2011), The climate effects of high latitude eruptions: The role of the time of year, *J. Geophys. Res.*, *116*, D01105, doi:10.1029/2010JD014448.

Kravitz, B., A. Robock, L. Oman, G. Stenchikov, and A. B. Marquardt (2009), Sulfuric acid deposition from stratospheric geoengineering with sulfate aerosols, *J. Geophys. Res.*, *114*, D14109, doi:10.1029/2009JD011918.

Kravitz, B., A. Robock, A. Bourassa, and G. Stenchikov (2010), Negligible climatic effects from the 2008 Okmok and Kasatochi volcanic eruptions, *J. Geophys. Res.*, *115*, D00L05, doi:10.1029/2009JD013525.

Llewellyn, E. J., et al. (2004), The OSIRIS instrument on the Odin spacecraft, *Can. J. Phys.*, *82*, 411–422, doi:10.1139/p04-005.

Mattis, I. (1996), Zeitliche Entwicklung des stratosphärischen Aerosols nach dem Ausbruch des Pinatubo: Analyse von Raman-Lidarmessungen (Temporal development of the stratospheric aerosol after the eruption of Mt. Pinatubo: Analysis of Raman lidar observations), diploma thesis, Univ. Leipzig, Leipzig, Germany.

Mattis, I., A. Ansmann, D. Althausen, V. Jaenisch, U. Wandinger, D. Müller, Y. F. Arshinov, S. M. Bobrovnikov, and I. B. Serikov (2002a), Relative humidity profiling in the troposphere with a Raman lidar, *Appl. Opt.*, *41*, 6451–6462, doi:10.1364/AO.41.006451.

Mattis, I., A. Ansmann, D. Müller, U. Wandinger, and D. Althausen (2002b), Dual-wavelength Raman lidar observations of the extinction-to-backscatter ratio of Saharan dust, *Geophys. Res. Lett.*, *29*(9), 1306, doi:10.1029/2002GL014721.

Mattis, I., P. Siefert, D. Müller, M. Tesche, A. Hiebsch, T. Kanitz, J. Schmidt, F. Finger, U. Wandinger, and A. Ansmann (2010), Volcanic aerosol layers observed with multiwavelength Raman lidar over central Europe in 2008–2009, *J. Geophys. Res.*, *115*, D00L04, doi:10.1029/2009JD013472.

McKeen, S. A., S. C. Liu, and C. S. Kiang (1984), On the chemistry of stratospheric SO_2 from volcanic eruptions, *J. Geophys. Res.*, *89*(D3), 4873–4881, doi:10.1029/JD089iD03p04873.

McLinden, C. A., J. C. McConnell, C. T. McElroy, and E. Griffioen (1999), Observations of stratospheric aerosol using CPFM polarized limb radiances, *J. Atmos. Sci.*, *56*, 233–240, doi:10.1175/1520-0469(1999)056<0233:OOSAUC>2.0.CO;2.

Müller, D., U. Wandinger, and A. Ansmann (1999), Microphysical particle parameters from extinction and backscatter lidar data by inversion with regularization: Simulation, *Appl. Opt.*, *38*(12), 2358–2368, doi:10.1364/AO.38.002358.

Oman, L., A. Robock, G. L. Stenchikov, G. A. Schmidt, and R. Ruedy (2005), Climatic response to high-latitude volcanic eruptions, *J. Geophys. Res.*, *110*, D13103, doi:10.1029/2004JD005487.

Oman, L., A. Robock, G. L. Stenchikov, T. Thordarson, D. Koch, D. T. Shindell, and C. Gao (2006a), Modeling the distribution of the volcanic aerosol cloud from the 1783–1784 Laki eruption, *J. Geophys. Res.*, *111*, D12209, doi:10.1029/2005JD006899.

Oman, L., A. Robock, G. L. Stenchikov, and T. Thordarson (2006b), High-latitude eruptions cast shadow over the African monsoon and the flow of the Nile, *Geophys. Res. Lett.*, *33*, L18711, doi:10.1029/2006GL027665.

Rault, D., and R. Loughman (2007), Stratospheric and upper tropospheric aerosol retrieval from limb scatter signals, *Proc. SPIE Int. Soc. Opt. Eng.*, *6745*, 674509, doi:10.1117/12.737325.

Read, W. G., L. Froidevaux, and J. W. Waters (1993), Microwave Limb Sounder measurement of stratospheric SO_2 from the Mt. Pinatubo volcano, *Geophys. Res. Lett.*, *20*, 1299–1302, doi:10.1029/93GL00831.

Ritter, C., A. Kische, and R. Neuber (2004), Tropospheric aerosol characterized by a Raman lidar over Spitsbergen, paper presented at 22nd International Laser Radar Conference, Eur. Space Agency, Matera, Italy.

Robock, A. (2000), Volcanic eruptions and climate, *Rev. Geophys.*, *38*, 191–219, doi:10.1029/1998RG000054.

Robock, A., T. Adams, M. Moore, L. Oman, and G. Stenchikov (2007), Southern hemisphere atmospheric circulation effects of the 1991 Mount Pinatubo eruption, *Geophys. Res. Lett.*, *34*, L23710, doi:10.1029/2007GL031403.

Russell, G. L., J. R. Miller, and D. Rind (1995), A coupled atmosphere-ocean model for transient climate change, *Atmos. Ocean*, *33*, 683–730.

Schmale, J., et al. (2010), Aerosol layers from the 2008 eruptions of Mt. Okmok and Mt. Kasatochi: In-situ UT/LS measurements of sulfate and organics over Europe, *J. Geophys. Res.*, *115*, D00L07, doi:10.1029/2009JD013628.

Schmidt, G. A., et al. (2006), Present day atmospheric simulations using GISS ModelE: Comparison to in situ, satellite and reanalysis data, *J. Clim.*, *19*, 153–192, doi:10.1175/JCLI3612.1.

Schuster, G. L., O. Dubovik, and B. N. Holben (2006), Angstrom exponent and bimodal aerosol size distributions, *J. Geophys. Res.*, *111*, D07207, doi:10.1029/2005JD006328.

Seinfeld, J. H., and S. N. Pandis (2006), *Atmospheric Chemistry and Physics: From Air Pollution to Climate Change*, 1203 pp., John Wiley, Hoboken, N. J.

Stenchikov, G. L., I. Kirchner, A. Robock, H.-F. Graf, J. C. Antuña, R. G. Grainger, A. Lambert, and L. Thomason (1998), Radiative forcing from the 1991 Mount Pinatubo volcanic eruption, *J. Geophys. Res.*, *103*, 13,837–13,857, doi:10.1029/98JD00693.

Stothers, R. B. (1996), Major optical depth perturbations to the stratosphere from volcanic eruptions: Pyrheliometric period, 1881–1960, *J. Geophys. Res.*, *101*, 3901–3920, doi:10.1029/95JD03237.

Stothers, R. B. (1997), Stratospheric aerosol clouds due to very large volcanic eruptions of the early twentieth century: Effective particle sizes and conversion from pyrheliometric to visual optical depth, *J. Geophys. Res.*, *102*(D5), 6143–6151, doi:10.1029/96JD03985.

Tang, I. N. (1996), Chemical and size effects of hygroscopic aerosols on light scattering coefficients, *J. Geophys. Res.*, *101*(D14), 19,245–19,250, doi:10.1029/96JD03003.

Tukiainen, S., S. Hassinen, A. Seppala, H. Auvinen, E. Kyrola, J. Tamminen, C. Haley, N. Lloyd, and P. Verronen (2008), Description and validation of a limb scatter retrieval method for Odin/OSIRIS, *J. Geophys. Res.*, *113*, D04308, doi:10.1029/2007JD008591.

Wandinger, U., A. Ansmann, J. Reichardt, and T. Deshler (1995), Determination of stratospheric aerosol microphysical properties from independent extinction and backscattering measurements with a Raman lidar, *Appl. Opt.*, *34*(36), 8315–8329, doi:10.1364/AO.34.008315.

Yang, K., X. Liu, P. K. Bhartia, N. A. Krotkov, S. A. Carn, A. J. Krueger, E. Hughes, R. J. D. Spurr, and S. G. Trahan (2010), Direct retrieval of sulfur dioxide amount and altitude from spaceborne hyper-spectral UV measurements: Theory and application, *J. Geophys. Res.*, *115*, D00L09, doi:10.1029/2010JD013982.

J. E. Barnes, Mauna Loa Observatory, National Oceanic and Atmospheric Administration Earth System Research Laboratory, 1437 Kilauea Ave., Hilo, HI 96720, USA.

L. Bitar and T. J. Duck, Department of Physics and Atmospheric Science, Dalhousie University, Halifax, NS B3H 3J5, Canada.

A. Bourassa, Department of Physics and Engineering Physics, University of Saskatchewan, 116 Science Pl., Saskatoon, SK S7N 5E2, Canada.

T. Deshler, Department of Atmospheric Science, University of Wyoming, Dep. 3038, 1000 E. University Ave., Laramie, WY 82071, USA.

F. Finger and I. Mattis, Leibniz Institute for Tropospheric Research, Permoserstr. 15, D-04318 Leipzig, Germany.

A. Hoffmann and C. Ritter, Alfred Wegener Institute for Polar and Marine Research in the Helmholtz Association, Telegrafenberg A45, D-14473 Potsdam, Germany.

B. Kravitz, Department of Global Ecology, Carnegie Institution for Science, 260 Panama Street, Stanford, CA 94305, USA. (bkravitz@carnegie.stanford.edu)

A. Robock, Department of Environmental Sciences, Rutgers University, 14 College Farm Rd., New Brunswick, NJ 08901-8551, USA.

D. Wu, Key Laboratory of Atmospheric Composition and Optical Radiation, Chinese Academy of Sciences, 350 Shushahu Rd., Hefei, Anhui 230031, China.